ENGINEERING APPLICATIONS OF COMPUTATIONAL FLUID MECHANICS
2024, VOL. 18, NO. 1, 2395452
https://doi.org/10.1080/19942060.2024.2395452

Taylor & Francis
Taylor & Francis Group

OPEN ACCESS Check for updates

3D computational fluid dynamics analysis of natural gas separation efficiency in multiphase pumping wells with heterogeneous flow regime

Charles C. Okafor and Patrick G. Verdin

Energy and Sustainability, Cranfield University, Cranfield, UK

ABSTRACT

This research uses 3D Computational Fluid Dynamics (CFD) simulations to investigate the downhole Natural Gas Separation Efficiency (NGSE) for multiphase pumping wells in the heterogeneous churn flow regime. Results explain the effects of key parameters such as liquid viscosity, intake port sizes/diameter, and casing diameter, on the NGSE. Methods are thus suggested to enhance the NGSE in oil field operations, and key improvements to the widely used mathematical formulations for viscous service are proposed. Transient numerical simulations were performed for a section of an experimental flow loop extracted from the literature, and the flow solution was obtained with the Volume of Fluid (VOF) model. For most simulations, turbulence effects were modelled with the $k-\varepsilon$ turbulence model. The $k-\omega$ SST turbulence model was however considered for the sensitivity analysis on liquid viscosity. The final numerical results validated against the corresponding experimental data showed an average error of less than 6%. Combining past literature and current results confirms that (i), the NGSE is affected by the downhole geometry (i.e annulus space and pump intake port flow area geometry) and (ii), current analytical NGSE models are not ideal for multiphase viscous service (high viscosity Newtonian flow) in the heterogeneous flow regime. The widely used steady-state formulations might thus not be adequate for this flow regime.

ARTICLE HISTORY
Received 8 April 2024
Accepted 17 August 2024

KEYWORDS
Electrical submersible pump (ESP); natural gas separation efficiency; 3D CFD; multiphase flow regime; viscous service; artificial lift

Nomenclature

A	Area (m^2)
A_{nn}	Total Annulus-A Area (m^2)
A_p	Total Pump intake port area (m^2)
D_c	Inner diameter of production casing
D_s	Outer diameter of DH ESP equipment
D_t	Outer diameter of the tubing
E_1	Average error
$\vec{F}_i$	External Body Forces
$\vec{F}_{ilift}$	Lift force
$\vec{F}_{itd}$	Turbulent dispersion force
$\vec{F}_{ivm}$	Virtual mass f0orce
$\vec{F}_{iwl}$	Wall lubrication force
g	Gravity (m/s^2)
GLR	Gas Liquid Ratio (Sm^3/sm^3)
Gp	Cumulative Gas $= \sum Q_{gt}\ \mathrm{dt}$
J_i	Superficial velocity of the i^{th} phase
J_{sl}	Superficial velocity of the liquid i^{th} phase
lb	Pound
m_{ij}	Mass transfer rate from i to j phase
m_{ji}	Mass transfer rate from j to i phase
P	Static Pressure (Pa)
P_{ann}	Pressure at Annulus-A outlet (Mpa)
P_b	Bubble pressure (Pa)
P_{ip}	Inlet Pressure into CFD model
P_p	Pressure at the Pump outlet (Mpa)
Q_{gt}	Total gas rate (Sm^3/d)
Q_{gp}	Gas rate into pump (Sm^3/d)
Q_{gv}	Gas vented rate (Sm^3/d)
Q_i	Total flow rate of the ith phase
Q_l	Liquid rate (Sm^3/d)
Re_{2ph}	2-Phase mixture Reynolds number
$\vec{R}_{ij}$	Interaction force between phases
S_i	Source term for phase i
S_r	Slip ratio
$\vec{v}$	Fluid velocity vector
V_∞	Terminal velocity (m/s)
$\vec{v}_i$	Velocity vector for ith phase
$\vec{v}_{ji}$	Interphase velocity
$V^P_{rs_g}$	Superficial gas velocity into the pump (m/s)
$V^i_{zs_g}$	Superficial gas velocity from Annulus (m/s)

Symbols & Abbreviations

α	Gas void fraction
β	Gas Volume Fraction (%) / volumetric quality

CONTACT Patrick G. Verdin p.verdin@cranfield.ac.uk Energy and Sustainability, Cranfield University, Cranfield MK43 0AL, UK

© 2024 The Author(s). Published by Informa UK Limited, trading as Taylor & Francis Group.
This is an Open Access article distributed under the terms of the Creative Commons Attribution License (http://creativecommons.org/licenses/by/4.0/), which permits unrestricted use, distribution, and reproduction in any medium, provided the original work is properly cited. The terms on which this article has been published allow the posting of the Accepted Manuscript in a repository by the author(s) or with their consent.

ρ	Density (kg/m^3)
$\overline{\overline{\tau}}$	Stress tensor

Subscripts

g	Gas phase
i	ith phase
m	Mixture

Abbreviations

cp	Centipoise
EXPT	Experiment
Err	Error
ft	Feet
GVF	Gas volume fraction
IA	Interest Area
ID	Internal diameter
LL	Liquid level
OD	Outside diameter
Sm^3/d	Standard cubic metre per day
Tbg	Tubing
VOF	Volume of Fluid

1. Introduction

Most current oil producing fields need some form of Artificial lift system to unlock a well potential. One such major artificial lift group is based on pumping technology. In this group, the Electrical Submersible Pumps (ESP) and the Progressive Cavity Pump (PCP) dominate (Bates et al., 2004). This research study focuses on ESPs as they remain the major and most popular downhole pumping technology from small to large volume of production (Liang & El-Kadri, 2018). It is anticipated that, as technology advancements increase ESP run life, there will be a significant growth of ESP use worldwide within the next few years, and more ESP wells will be subjected to harsher environments (Anthony, 2017), which will include high gas volume fractions and viscous services (i.e. heavy oil production).

Most installed ESPs today provide full access to the Tubing – Casing annulus (Annulus–A) that permits gas venting. Unless the well is subjected to downhole packers, the ability to vent gas via the Annulus-A is a technique that should be adopted as much as possible to minimize the quantity of free gas dragged into the Pump. Access to the Annulus-A is advantageous as it permits downhole natural separation for the pumping wells, venting gas as much as possible as, if ingested into the pump, gas can be detrimental to pump operations (Ooo & Purneftegas, 2008), and eventually lead to full pump failure (Wilson, 1994).

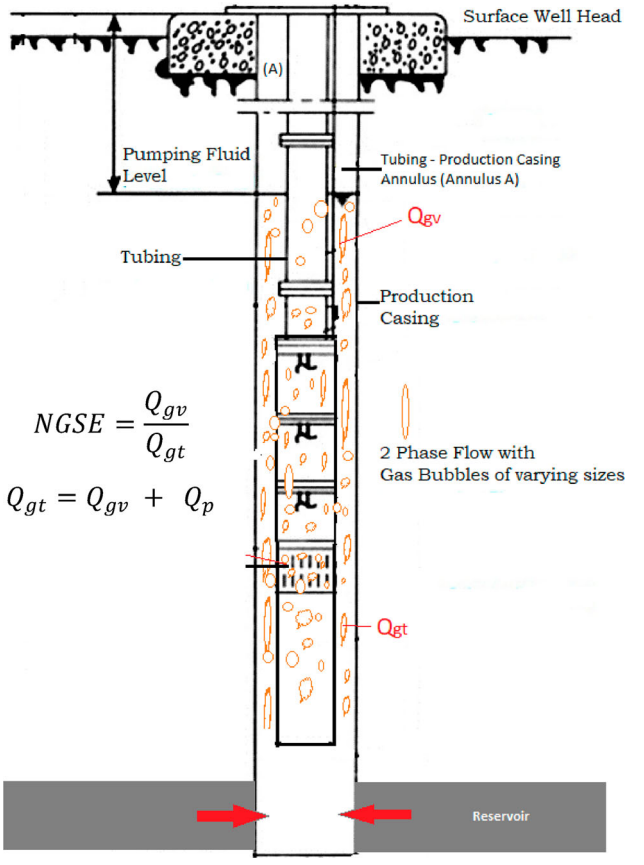


Figure 1. Two phases in a pumping ESP well (modified from Okafor et al., 2021).

When the pressure in the vicinity of the pump drops below the bubble point pressure under in-situ conditions, gaseous and liquid phases are present, see Figure 1. At such thermodynamic conditions, a quantity of free gas exists; part of it will be vented via the Annulus-A and the remainder will be dragged alongside the liquid into the pump (Liu & Prado, 2004). For most ESPs, this free gas dragged into the pump should remain below a certain threshold to prevent affecting pump head and efficiency (Pessoa & Prado, 2001), substantial downtime, and reduction on pump run life (Camilleri, 2020).

Best practice for ESP design and operational management is either stipulated as the gas fraction, which should remain below 35% (Krasnov et al., 2014; Ooo & Purneftegas, 2008), or the free gas dragged into the pump which should remain between 10–20% (Bagci et al., 2010). To achieve such challenging figures, it is recommended to always keep the Annulus-A accessible to gas venting via bottom hole natural separation. Otherwise, artificial gas devices may be needed, incurring extra cost to the installation (Hua et al., 2012; Ooo & Purneftegas, 2008).

In packerless completions, natural gas separation is an important part of the overall bottomhole gas separation process (Harun et al., 2001). Intuitively, it is defined

Table 1. Alhanati, 1993 Experimental Set up (∗ assumed, based on the first author's field experience with ESPs).

Breakdown of the 15.24 m experimental Casing Section (Alhanati, 1993)				
Item	Equipment	Description of equipment	ID (m)	Length (m)
1	0.1778m (7inch) Production Casing	34.2 kg/m weight	0.1615	15.24
2	3.66 m motor housing	400 series dummy motor	0.0762	3.66
3	Pump Intake or Rotary Gas Separator (RGS)	∗ 400 series RGS (6 port holes size 16–17 mm)	0.0762	1.22
4	2.04 m Dummy ESP housing	400 series- No Stages: No impellers, No Diffusers	0.0762	6.71
5∗	0.089 m (3.5inch) Tubing & Cross Over	0.09 m Cross Over & Tubing, 13.8 kg/m	0.0759	0.61

as the ratio of free gas vented (Q_{gv}) to the available free gas in the pump casing annulus (Q_{gt}). The Natural Gas Separation Efficiency (NGSE) could be affected by many factors, such as annulus area, flow rate, fluid properties, buoyancy, gravitational effects, and downhole geometry of the pump (Liu & Prado, 2004; Marquez & Prado, 2003). With more ESPs now subjected to challenging gas environments, it becomes extremely important to revisit past research on NGSE, identify past and new challenges, knowledge gaps, utilizing recent advances in computational power and numerical methods though Computational Fluid Dynamics (CFD).

The investigation of the downhole Natural Gas separation began in 1980 with Lea and Bearden (1982) who studied the experimental effects of free gas on centrifugal submersible pumps using air and water as the working fluids. As part of their investigation, they reported a separation effect where free gas was vented via the annulus. Regarding natural annulus separation effects, they concluded that the NGSE increased as gas quantity increased (Harun et al., 2000) and with a lower pumping liquid rate, the NGSE increased. These experiments were conducted with a fixed casing size, and fixed fluid properties, pressure, and temperature.

Alhanati (1993)'s experimental research confirmed the above findings. A 15.24 m (50 ft) vertical research facility comprising a dummy motor, pump housing in a 0.178 m (7")

OD casing (0.162 m, ID) was built for studying the efficiency of a rotary gas separator, as summarized in Table 1.

Using air and water as the working fluids and with an overall gas void fraction (volumetric quality) between 0.61 and 0.70, Alhanati estimated the NGSE using Equation (1), for eight data points (c.f. Table 2), when the rotary gas separator was switched off.

$$NGSE = \frac{Q_{gv}}{Q_{gt}} \tag{1}$$

where Q_{gv} and Q_{gt} are the free gas vented, and the total available free gas in the pump casing annulus.

The annulus separation effects were investigated under two sets of operating conditions: approximate liquid flow rates of 95.4 and 143.1 Sm^3/d, and gas–liquid ratios (GLR) of 17.8 and 35.6 Sm^3/Sm^3 (Alhanati et al., 1994). To enhance data analysis, we calculated the overall gas volume fraction (GVF) at the respective thermohydraulic condition for each experiment and incorporated this parameter into Table 2 (Column G).

Alhanati proposed a uniform void fraction simplified drift flux model shown in Equation (2), for estimating the NGSE.

$$NGSE = \frac{V_\infty (1-\alpha)^n}{V_\infty (1-\alpha)^n + J_{sl}} \tag{2}$$

where V_∞ is the terminal velocity of the gas, α the gas void fraction, and $J_{sl}$the superficial liquid velocity. The numerator in Equation 2 is a simplified expression of the drift velocity. Both this drift velocity and the exponent n are flow regime dependent (Hibiki & Ishii, 2002; Isao & Mamoru, 1987). As reported by Liu and Prado (2005), n can be taken as 0 for both slug and churn flows. When buoyancy and gravity separation is dominant, the terminal velocity V_∞can be calculated with Equation 3 (Hibiki & Ishii, 2002).

$$V_\infty = 1.414\left[\frac{\sigma(\rho_l - \rho_g)g}{{\rho_l}^2}\right]^{1/4} \tag{3}$$

where σ is the surface tension, g the gravity term, and ρ the density, with the subscripts l and g denoting liquid and gas, respectively.

Equation (2) is applied in most major current steady state ESP design and operation software due to its ease of application. However, it is important to highlight the drawbacks of this model, which assumes a turbulent flow regime (Hibiki & Ishii, 2002) and a uniform gas void fraction (Harun et al., 2000) from the bottom of the ESP motor up to the pump intake. This assumption of uniform gas void fraction considers no slippage between the gas and the liquid phases and hence the GVF estimated in Table 2 is an approximate estimation of the uniform gas void fraction suitable for Equation (2). However, research by Shi et al. (2005) on two-phase flows in wellbores using Gamma and Electric probes nullifies this assumption, as the authors clearly showed the effect of slippage and varying gas void fraction in a similar shorter pipe system of 11 m.

In 1994, further experiments were conducted by Sambangi using air and water. Liquid flow rates from

Table 2. Alhanati, 1993 experimental results: modified to SI units, from Alhanati and Schmidt.

	T	*P*	Ql	Qgt	Qgv	(GVF)	GLR	NGSE
Run	°C	Kpa	Sm^3/d	Sm^3/d	Sm^3/d	(%)	Sm^3/Sm^3	%
A	B	C	D	E	F	G	H	I
19	38.3	834	102	1444	903	61.1	14.2	62.5
20	38.3	841	153	2331	1181	63.0	15.2	50.7
21	36.7	793	634	3381	2152	79.5	5.3	63.7
22	33.9	752	912	4993	2197	80.7	5.5	58.4
23	34.4	1510	614	1696	810	52.1	2.8	47.7
24	39.4	1607	877	2563	1113	52.7	2.9	43.4
25	38.8	1517	631	3324	1835	67.7	5.3	55.2
26	36.7	1379	915	4996	2330	70.5	5.5	46.7

95.4 to 476.9 Sm^3/d, with GLRs of 8.9, 17.8, 35.6 and 53.43 Sm^3/Sm^3, were investigated in a similar vertical experimental set up as used previously by Alhanati (Marquez & Prado, 2003). Even though additional data were gathered, no significant modifications were proposed to the Alhanati simplified model (Harun et al., 2000).

In 1997, Lackner investigated NGSE using mineral oil and air. The objective was to study experimentally the influence of fluid physical properties on the downhole separation process (Lackner, 1997). The argument was that hydrocarbon fluids do not behave like air–water, under identical conditions, as density, surface tension and viscosity are different due to their chemical composition. Liquid viscosity was the main emphasis of the investigation with values ranging from (1.1 to 50) mPa·s at 37.8°C. It was shown that for the extent of the viscosity investigated, there was a negligible influence on the NGSE due to the flow still been characterized by turbulence, and Alhanati's model was still valid (Harun et al., 2000). A key statement here is that the flow was Newtonian and stayed turbulent.

A new addition to the NGSE knowledge was through the experimental work by Serrano (1999), who investigated the effect of inclination angle to the NGSE at lower GVF. The investigation endorsed the influence of flow regime on the NGSE, as most of Serrano's experiments were carried out in the bubble flow regime (Marquez & Prado, 2009). Serrano showed that an increase in liquid and gas rates both decrease the NGSE. He also concluded that changes in pressure had a negligible effect on the NGSE and the Alhanati simplified mathematical model was not valid for void fractions less than 20% (Harun et al., 2000).

In the early 2000s, several analytical modelling studies on NGSE appeared in the literature. Most researchers used data from experimental studies of Alhanati (1993), Sambangi (1994), Lackner (1997) and Serrano (1999) to propose various modifications of the drift flux model to estimate the NGSE. Harun et al. (2000) assumed a uniform void fraction across the annulus and proposed a drift flux model based on combined phase momentum equations to estimate the NGSE in vertical pumped wells, and a relative velocity closure relationship that incorporates a new drag correlation corresponding to the bubbly and churn flow regimes. In 2001 this model was improved further towards deviated wells (Harun et al., 2001) with the inclusion of a new in-situ/local void fraction correlation and a drag coefficient that were both flow pattern dependent.

More recently, the ESP community has adopted the Marquez and Prado (2003) model. This model has been identified in the literature to be an improvement from all previous drift flux models (Shakirov, 2011) as the formulation considers a slip velocity in both vertical and radial directions. However, a major drawback of the model is its inability to replicate the effects of increasing NGSE with increasing gas volume. The simplified form of the Marquez and Prado (2003) model can be found in Equation (4), where $V^P_{rs_g}$ is the superficial velocity of the gas into the pump, $V^i_{zs_g}$ is the superficial velocity of the gas from the Annulus-A, A_p is the total area of the Intake port holes and A_{nn} is the area on the Annulus-A. This equation considers the downhole geometric characteristics of the pump intake flow area (diameter of the Pump Intake Ports) in relation to the Annulus-A (Marquez & Prado, 2003).

$$NGSE = \frac{Q_{gv}}{Q_{gt}} = 1 - \frac{V^P_{rs_g}}{V^i_{zs_g}} \frac{A_p}{A_{nn}} \tag{4}$$

The authors claimed that the ability to resolve Equation 4 is wholly dependent on the quantity of gas going into the pump intake. In addition, when compared with the Tulsa University Artificial Lift Projects (TUALP) experimental databank, although still significant, an absolute error of 15.24% was obtained, which was an improvement over Alhanati's model absolute error of 25.64%.

The most recent work from Marquez and Prado (2009) investigated the NGSE based on vorticity stream function

using 2D cylindrical coordinates. This approach considers the flow regime and conservation equations for two-phase flows via a two-phase model. The model proposes the estimation of the gas void fraction at the pump intake, with a new term called the 'interface characteristic length'. New correlations were then proposed for the interface characteristic length, which is highly dependent on the thermohydraulic conditions and the flow regime. This two-phase model was used to investigate the effects of casing size, GLR, and liquid viscosities from 1 mPa·s to 50 mPa·s on the NGSE (Marquez & Prado, 2009). Results showed that within the viscosity range studied for bubble, slug, and churn flow regimes, increasing the viscosity decreases the NGSE. However, these results contradict experimental research from Lackner (1997) where at similar temperatures (37.8°C), viscosity was increased from 1 mPa·s to 50 mPa·s and showed little influence on the NGSE.

Building on the work of Marquez and Prado (2009), Okafor et al. (2021) employed a 3D VOF CFD model to study NGSE in churn flow. Their work offers valuable insights for improving viscous service modelling and understanding the impact of intake port area (A_p) on the NGSE. However, their study was limited and did not validate existing void fraction correlations, particularly for scenarios with higher liquid viscosities, against modern CFD methods or laboratory data. Additionally, it lacked specific guidance for ESP vendors on minimizing port hole effects on NGSE. These limitations suggest future research directions.

Table 3 summarizes recent progress in Natural Gas Separation Efficiency (NGSE) research. As shown in Table 3, most of the work published to date has focused on experimental and theoretical studies. In the authors best knowledge, there has been scarce work published in the public domain on utilizing 3D CFD modelling to study the NGSE, apart from the studies of Okafor et al. (2021) investigating the NGSE in churn flow, particularly for scenarios with higher liquid viscosities.

2. Knowledge summary and gaps

While significant advancements have been made, challenges remain in this area of research.

2.1. Known information

Alhanati's experiments established void fraction ranges for slug and churn flows ($0.25 < \alpha < 0.70$), while Serrano's work focused on the bubble flow regime ($\alpha < 0.20$) (Harun et al., 2001; Marquez & Prado, 2009). Some studies report various void fraction cut-off ranges for example bubble flow at even lower void fractions, highlighting the need for further investigations (Ghiaasiaan, 2007; Guo et al., 2018; Hasan et al., 2007).

A key contribution of Serrano's research was to distinguish the NGSE based on flow regimes. Previously, Alhanati's work explored the heterogeneous regime, whereas Serrano focused on the homogeneous regime. This distinction is crucial for accurate modelling of the NGSE behaviour, which requires flow regime-dependent closure relations for parameters like interfacial area and drift velocities. Additionally, selecting the appropriate multiphase CFD model hinges on the identified flow regime.

Downhole geometry significantly impacts NGSE (Harun et al., 2000; Marquez & Prado, 2009). Specific aspects like the casing annulus hydraulic diameter and intake port diameter influence separation efficiency (Marquez & Prado, 2003).

The NGSE is dependent on fluid properties (gas density, viscosity, etc), operating pressure and possibly thermodynamic conditions (Lea & Bearden, 1982). Comparable effects were studied in similar industrial multiphase processes such as bubble columns (Besagni et al., 2018; Nedeltchev & Schumpe, 2008).

2.2. Research gaps

Although improved with the inclusion of a slip in the radial axis, the widely used Marquez and Prado (2003) 2D simplified drift flux mechanistic model carries a percentage error circa 20–22% when compared with experimental data in the heterogeneous regime, as highlighted in Figure 2. Clusters B and C in this figure, have higher absolute error (circa 21%) than data in Cluster A. Cluster C shows mostly data in the heterogeneous flow regime (Marquez & Prado, 2009). It should be noted that during the ESP design phase, an absolute error of 22% could lead to additional costs of the installation, with the purchasing of a rotary gas separator, gas handler, or a multiphase pump. As illustrated through Table 4, if a hypothetical case using Experiment 19 from Table 2 is considered, the case of 21% error on the NGSE is shown to overpredict the Free Gas into Pump (FGIP). In this case, a gas handler might have to be installed to abide by the industry 10-20% FGIP rule (Bagci et al., 2010). Such a situation may lead to extra cost or the underpredicting of the NGSE, resulting in gas troubles or reduction of ESP run life. Hence more work and best field practices are needed for enhancing estimations and managing operations in the heterogeneous flow regime. The practicing engineer should consider these possibilities.

Table 5 identifies the possibility for each currently used analytical model to reproduce experimental results and areas with no conclusive experimental data. For instance,

Table 3. Summarizing the public literature.

Research type	Researchers	Year	Summary
Experimental Investigation	Lea and Bearden	1980	Concluded that increased gas content amplified the NGSE (Lea & Bearden, 1982).
	Alhanati	1993	Investigated the NGSE at gas void fractions > 20% (Harun et al., 2000).
	Sambangi	1994	Expanded the experimental window of Alhanati's experiments to validate the existing analytical model (Harun et al., 2000).
	Lackner	1997	Researched the effect of liquid viscosity on the NGSE. (Harun et al., 2000; Liu & Prado, 2004).
	Serrano	1999	Investigated the NGSE at Gas void fractions < 20%. (Harun et al., 2000)
Theoretical Research	Alhanati	1993	A simplified drift flux equation to estimate the NGSE. In situ gas void fraction is assumed constant (Alhanati, 1993).
	Serrano	1999	Developed a correlation to estimate in situ void fraction from the gas volume fraction (Harun et al., 2001; Marquez & Prado, 2003).
	Harun et al.	2000, 2001	Drift flux approach with the 1992 void fraction correlation of Hassan and Kabir (Harun et al., 2001, 2000)
	Bin Liu	2001	Research on the NGSE via the Vorticity stream function approach (Liu & Prado, 2004).
	Marquez and Prado	2003	Drift Flux model via 2D cylindrical coordinates. The inclusion of slip in the radial direction (Marquez & Prado, 2003).
	Marquez and Prado	2009	Two Fluid Model based on vorticity stream function using 2D cylindrical coordinates (Marquez & Prado, 2003).
3D Numerical Research	Okafor et al.	2021	The first attempt using 3D CFD numerical simulations, the VOF multiphase model to study the NGSE (Okafor et al., 2021).

Table 4. 21% error illustration on the NGSE.

Total fluid **(m^3)**		Gas (m^3)	GVF	Liquid (m^3)	Liquid volume		
1431		**620**	**43%**	**811**	**57%**		
Metered				**21% Error**			
Qgv	**Qgp**	**NGSE**	**FGIP**	**NGSE**	**Qgv**	**Qgp**	**FGIP**
m^3	m^3	%	%	Error	m^3	m^3	(%)
391	230	63	16	50%	309	312	22
No gas troubles				Possible gas troubles			

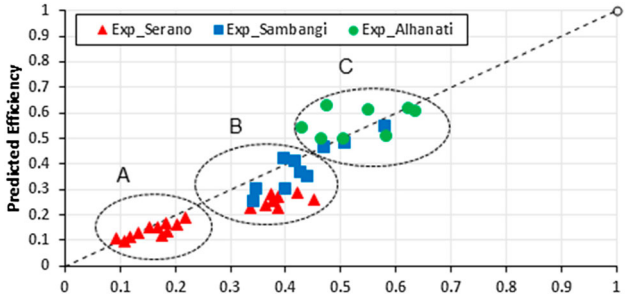


Figure 2. Measured vs Predicted efficiency (modified from Marquez and Prado (2003)).

there has been no NGSE laboratory experiments carried out to date, to physically explore the change of geometry, Pump Intake Port area, or changes in the Annulus Hydraulic Diameter (casing diameter increase with fixed tubing size); such experiments would be costly and published works have not suggested methods to further improve the area of port hole design by providing specific guidance for ESP vendors on how to minimize port hole effects on NGSE.

Another lack of knowledge is regarding the liquid viscosity (Marquez & Prado, 2003). While Marquez and Prado (2009) conducted viscosity sensitivity studies (1–50 mPa·s) that yielded results differing from those of Lackner (1997) at 37.8°C. Okafor et al. (2021) partially addressed this by reproducing Lackner's findings and suggesting viscosity affects beyond 50 mPa·s. However, a critical gap remains: the lack of comprehensive validation for proposed corrections to Equation (2) in viscous service conditions. Further research is necessary to establish and validate reliable correlations for liquid viscosity effects on NGSE.

The increasing availability of computational power has fuelled the popularity of 3D numerical simulations for multiphase flow studies (Itou et al., 2005). While computational costs can be significant, 3D CFD has become a mature technology with widespread applications in fluid dynamics and engineering (He et al., 2022). CFD continues to gain popularity in the oil and gas sector, allowing for extensive parametric studies that would be impractical through experiments alone.

This study extends the foundational CFD work of Okafor et al. (2021). 3D CFD simulations are used to conduct a comprehensive investigation of the NGSE, and meticulously detail the concepts behind the flow models selection, validation against Alhanati's (1993) experimental data, and highlight the results of simulated

Table 5. Knowledge gaps- experiment and mathematical models.

Known gaps (experiments and models)							
		Analytical models					
Parameter	Experiments	Alhanati (1993)	Harun et al. (2000)	Harun et al. (2001)	Marquez and Prado (2003)	Marquez and Prado (2009)	Okafor et al. (2021)
GLR	Alhanati, Lea Bearden Sambangi	Y	N	N	Y	Y	*
Viscosity	Range (1.1 -50cp) No Experiments > 50cp	*	*	*	*	N**	N**
Pressure	Alhanati, Sambangi	N	N	*	N	N	*
Annular Diameter	No Experiments	Y	Y	Y	Y	N	Y
Intake port Area (Sizes)	No Experiments	*	*	*	Y	*	N**

N: A decrease in NGSE as the parameter increases
Y: An increase in NGSE with an increase in parameter.
*: No public records or research in the literature, **: No validation against experimental/simulation data

sensitivity analyses: surface tension and liquid density, as reported by Lackner (1997). Other key contributions are:

(a) Liquid Viscosity Impact: Identified a suitable gas void fraction correlation for correcting equation 2 and improved accuracy in viscous service.
(b) Downhole Geometry: Emphasized the significance of downhole geometry and introduced practical solutions for intake port flow area management.

These advancements greatly benefit NGSE research.

3. Methodology and validation

The 3D geometry design, meshing, and numerical simulations were performed with the ANSYS Workbench 2019R1 platform. The goal was to define a suitable replica of the Alhanati (1993) test rig, a fit-for-purpose geometry, mesh and select the appropriate multiphase model to describe the physics of the flow.

3.1. Laboratory set up description

A replica of the Alhanati, 1993 test rig is shown in Figure 3. This replica has been constructed from the published description of the experimental programme with the main components explained in Table 1.

The 15.24 m test rig was designed to reproduce a geometry of an ESP set up (D in Figure 3) at the bottom of the well, using a 6.71 m (22 ft) dummy pump housing and motor seal section (A+B in Figure 3) of 3.66 m (12 ft). At the top of the test rig, an electrical motor (E in Figure 3) was mounted above the pump discharge head. To complete the model, the authors assigned a 1.22 m pump intake/rotary gas separator (C in Figure 3).

Water and gas are fed from the bottom (Figure 3) at targeted gas liquid ratio (GLR) and gas vented at the top (F, Figure 3). All rates were measured and reported in standard conditions. The corresponding pressure, and

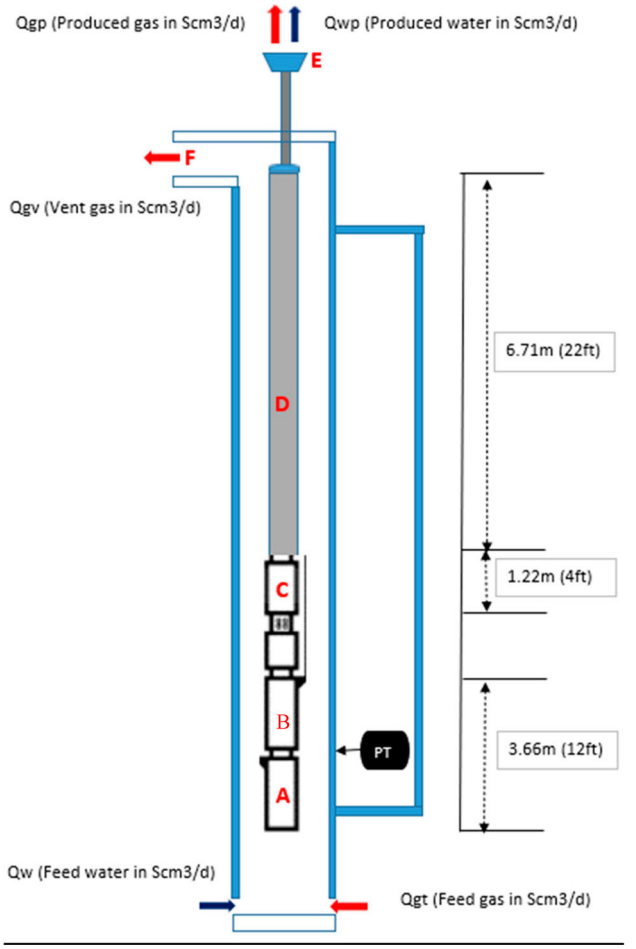


Figure 3. Replica of the Alhanati, 1993 test rig. (Not to scale).

temperature (PT) for each experiment were also reported as given in Table 2.

3.2. Geometry design and meshing

The 3D geometry was built using the equipment data in Table 1. This data is a breakdown of the equipment used by Alhanati in 1993, with Figure 3 defining the design for the CFD geometry shown in Figure 4. The flow domain

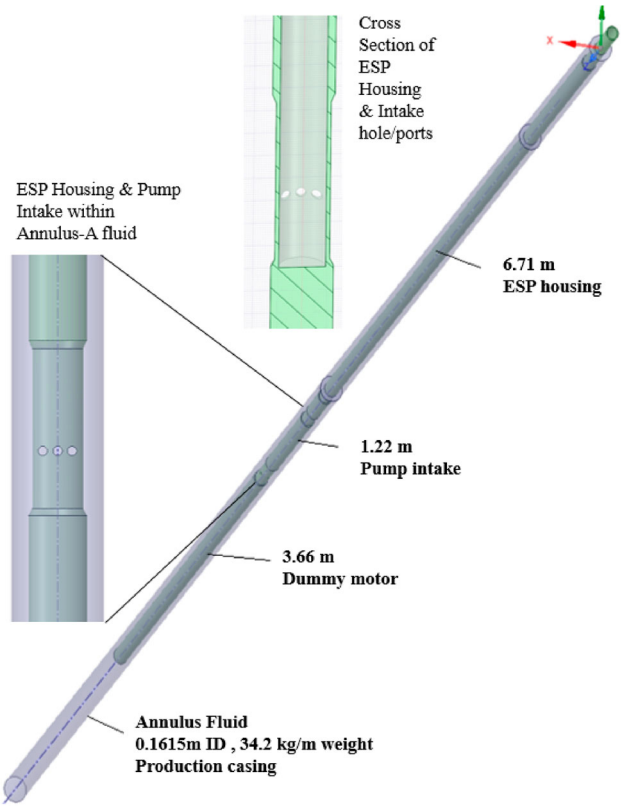


Figure 4. Geometry design for Alhanati, 1993s experiments (Modified from Okafor et al., 2021).

is a vertical 0.178 m diameter (ID 0.162 m), 34.2 kg/m weight production casing size of length 15.24 m. A 6.71 m dummy ESP with no impellers or diffusers is located inside the casing. As such, a setup of a 'Pipe-in-Pipe' system is obtained, with the ESP housing acting as a wall between two fluids: an internal fluid domain in the ESP housing and an external fluid domain in the Annulus-A.

As shown by the CFD geometry design in Figure 4, the domain consists of the 6.71 m ESP housing fluid, the annulus fluid path, and the 1.22 m pump intake. Based on the authors' expertise, the ESP motor is located 3.05 m from the bottom to enable sufficient distance for both phases to mix when injected from the bottom boundaries.

The ESP system under investigation features a 1.22 m diameter pump intake equipped with six (6) port holes for fluid entry. The intake sits above a 3.66 m dummy motor below the ESP housing. Fluid enters the ESP from the 0.178 m (7 in) casing annulus through these ports. Each port hole has an approximate diameter of 17 mm.

Figure 5 illustrates the workflow, encompassing the geometry design and mesh generation process. The ANSYS meshing software was used to create an unstructured mesh with approximately 5.2 million cells. Unstructured meshes offered flexibility, particularly for refining areas around the six-port hole entry points and near wall regions, crucial for accurate modelling, depending on the chosen turbulence model. This meshing approach achieved the closest model accuracy with the simulations and prevented convergence issues. To ensure grid independence, five additional meshes were generated by progressively upscaling the initial 5.2 million cell mesh.

3.3. Fluid properties & conditions

The model assumes immiscibility between both phases. Fluid rates from the experiment were reported at standard conditions (Table 2) and for simplicity in the numerical modelling (to prevent the uncertainty associated with the test rig measuring device and the conversion of in-situ rates to standard condition rates), mass rates were chosen as the feed rates into the CFD model. Fluid properties were then defined at standard conditions, and such aligns the simulated volume rates with the reported experimental rates.

3.4. Turbulence and near wall treatment

It is generally accepted that pipe flows in the oil industry are mostly turbulent. In this study (apart from the sensitivity analysis on viscosity), turbulence effects were

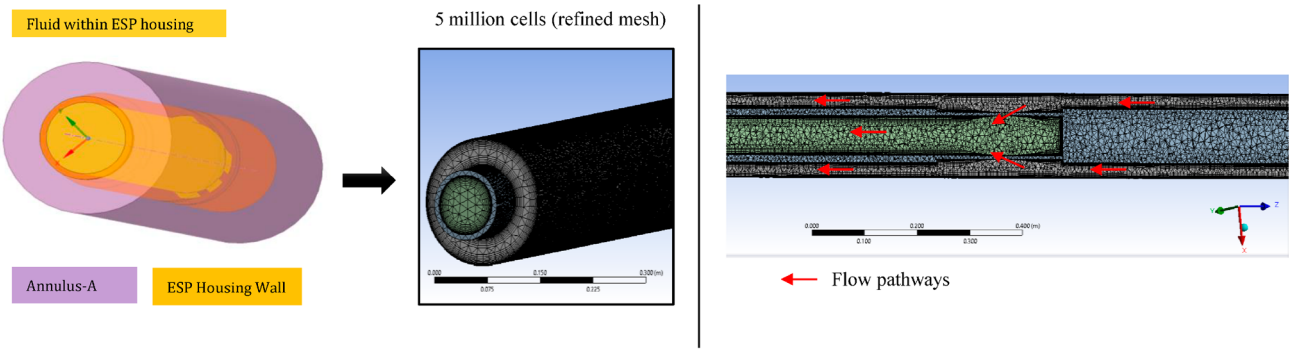


Figure 5. Geometry to refined Mesh. Cross section of mesh showing flow pathways.

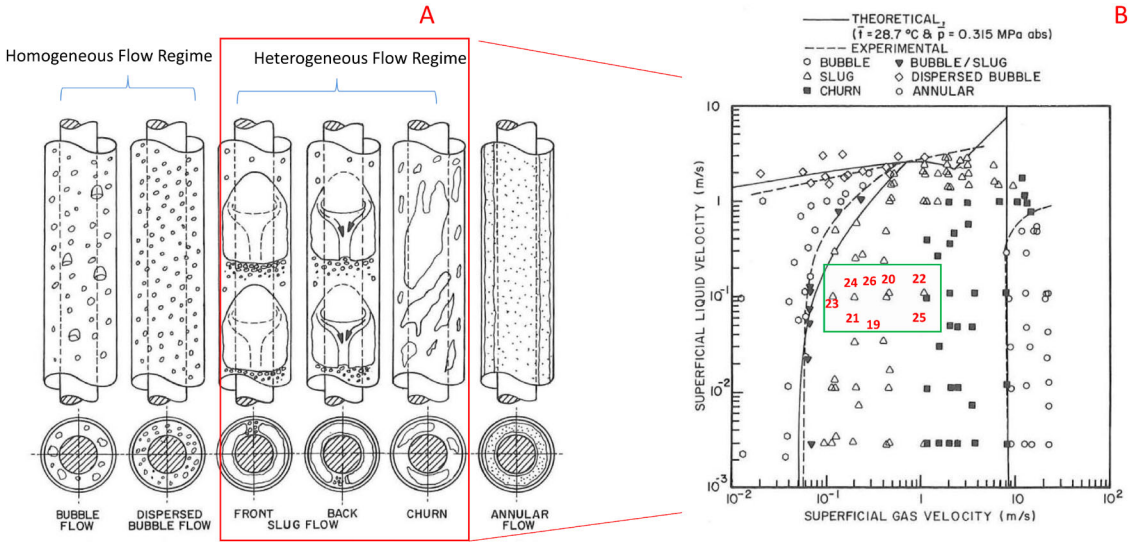


Figure 6. (A): Flow regimes for concentric annulus; (B): Flow regime map: air-water concentric annulus; The numbers in red font (green box) represent the approximate location of each experiment (23 represents Experiment 23 for instance). (Both figures are modified from Caetano et al., 1992).

modelled with the Reynolds Averaged Navier Stokes (RANS) $k-\varepsilon$ model. The transport equations for the turbulent kinetic energy (k) and the energy dissipation rate (ϵ) can be retrieved from the ANSYS Fluent Theory Guide (ANSYS, 2011). For the sake of clarity, they are reported in Appendix A1. Detailed description of this turbulence model can also be retrieved from Gourma and Verdin (2016).

The k – ϵ two-equation turbulence model offers a good compromise on numerical capabilities and computational accuracy (Gourma & Verdin, 2016). It can be inaccurate however, especially in case of large pressure gradients but is numerically stable and fast, so is widely used for industrial applications (Loyseau et al., 2018).

For most simulations in this work, the near-wall region was not of prime interest, and logarithmic-based wall functions were thus used to resolve the boundary layer and applied to achieve a non-dimensional distance at the wall $30 < y+ < 300$.

However, for the sensitivity analysis on viscosity, the k – ω SST with 'Low Reynolds Correction' was selected to capture transition and possible laminar flow areas, and hence a $y+ < 5$ was achieved at the walls (viscous sublayer resolving approach to resolve the boundary layer). This aspect will be elaborated further in the viscosity sensitivity section (Section 4). The k – ω SST turbulence model has been successfully used for similar applications, as reported in the literature, see Loyseau and Verdin (2016). Detailed description of the k – ω SST turbulence model can be retrieved from the ANSYS Fluent Theory Guide (ANSYS, 2011).

3.5. Multiphase flow regime and CFD flow model

Pump Intake Pressure (PIP) monitoring is a common practice for identifying two-phase flow regimes near ESPs (Camilleri, 2020; Pessoa & Prado, 2001). The flow regime in the annulus (Annulus-A) can then be categorized using maps like those developed by Caetano et al. (1992) for upward vertical flow in concentric annuli. We classify the flow regimes near ESPs to align with the homogeneous (dispersed bubble) or heterogeneous (slug/churn) regimes shown in Figure 6(A).

The concentric annulus superficial velocity of a fluid can be written as:

$$J_i = \frac{Q_i}{\pi (D_c^2 - D_s^2)/4} \tag{5}$$

where Q_i is the flow rate of the phase i, D_c is the inner diameter of the production casing, and D_s is the outer diameter of the downhole ESP equipment. With Equation (5) and Tables 1 and 2, the superficial velocities for both gas and liquid phases (J_g and J_l) were calculated and plotted on the Caetano et al. (1992) experimental flow map for two-phase air–water flow in concentric annuli systems (Figure 6B).

The identified heterogeneous flow regime in Figure 6(B) guided the selection for the Volume of Fluid (VOF) multiphase flow model using the industry standard CFD code ANSYS Fluent. Fully transient implicit 3D simulations were performed with the VOF multiphase flow model as this multiphase model has been widely used for various CFD analyses in the multiphase heterogeneous

flow regime (Guerrero et al., 2017; Ragab & Brandstaetter, 2008; Zhu & Zhang, 2018).

The VOF approach can model multiple immiscible fluids by solving a single set of momentum equations and tracking the volume fraction of each of the fluids throughout the domain (Gourma & Verdin, 2016, p. 2020). The continuity equation for VOF (ANSYS, 2011) written with the mixture density is:

$$\frac{1}{\rho_i}\left[\frac{\partial}{\partial_t}\rho_m + \nabla(\rho_m \vec{v}_i)\right] = S_{\alpha i} + \sum_{i=1}^{n}(\dot{m}_{ij} - \dot{m}_{ji}) \quad (6)$$

where ρi and $\vec{v}_i$, is the density and velocity vector of phase i, Sαi is a source term for phase i, and $\dot{m}_{ij}$ is the mass transfer from phase i to j (vice versa for $\dot{m}_{ij}$). The density of the mixture (ρ_m) is weighted by the volume fraction of each phase (Equation 7):

$$\rho_m = \sum_{i=1}^{n} \alpha_i \rho_i \quad (7)$$

The volume fractions of all phases should sum to unity.

Equation (8) describes the momentum equation for the VOF model (ANSYS, 2011). $\vec{F}$ is the surface tension force (modelled as a body force), P is the pressure and g the gravitational force. As this model solves a single momentum equation for both phases, an increase of momentum of any phase increases the overall fluid mixture velocity and hence, would not be valid for sensitivity simulations monitoring of individual phase velocities (i.e. increase in GLR effects).

$$\frac{\partial(\rho_m \vec{v})}{\partial_t} + \nabla(\rho_m \vec{v}\vec{v}) = -\nabla P + \nabla(\bar{\bar{\tau}}) + \rho\vec{g} + \vec{F} \quad (8)$$

3.6. Boundary conditions, initialization, monitoring

All numerical simulations were assumed isothermal, with temperature values taken from Table 2. A no-slip boundary condition was applied at all walls. One inlet and two outlets were considered, see Figure 7. A mass flow inlet type boundary condition was set-up at the inlet of the domain (Table 6: M_g and M_w), with gas and water injected at the bottom of the annulus, 3.05 m below the ESP dummy motor. A pressure outlet type boundary was applied at the ESP discharge (Outlet 1), as reported in Table 6 for each experiment. The ESP fluid outlet (Q_{gp}-Gas outlet from the ESP discharge) was monitored at this boundary. A pressure outlet type boundary condition was also considered for the Annulus-A (Outlet 2), where the gas outlet from the Annulus-A (Q_{gv}) was monitored. Initially this boundary mimicked a closed valve (wall-type condition), which was opened later in the simulation and

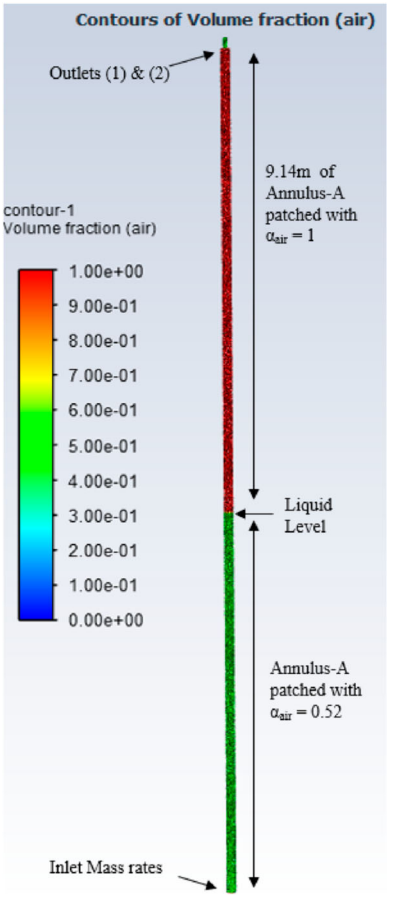


Figure 7. Initialized and patched GVF Experiment 23.

became subjected to a backpressure, with values shown in Table 6.

Using Experiment 23 as an example and Table 2, Figure 7 shows the initialized model with GVF = 0.52, below the liquid level (LL). Above LL, GVF = 1, this represents the gas filled Annulus-A in the downhole ESP system.

Three planes cut across the motor section located 5.5, 6.1 and 6.7 m far from the inlet of the system, were used for monitoring the numerical gas void fraction and fluid/phase velocities just below the pump intake, located 6.5 m far from the bottom (see Figure 17A). The 6.1 m cross-section plane termed 'Interest Area' (IA) hereafter, is located just before the Pump Intake Ports. Ideally, steady/stable parameter conditions at the IA should be obtained just before the liquid reaches the Annulus-A outlet.

3.7. Mesh independence study

A mesh independence study was performed to ensure that the results of the simulation did not depend on the mesh density. For this exercise and based on Equation (2), the cumulative gas vented was compared by increasing

Table 6. Summary of results for all 8 Alhanati, 1993 experiments.

Exp	Mw	Mg	Pp	Pann	Pip	Pip	NGSE	NGSE	|α|	Proposed Flow Regime
	Boundary conditions used in the NGSE models for Figure (9-16)				Expt	CFD	Expt	CFD	*	
A	B	C	D	E	F	G	H	I	J	K
Expt (E)	Kg/s	Kg/s	Kpa	Kpa	Kpa	Kpa	%	%		
E19	1.18	0.02	833	834	834	841	63	71	0.73	Churn
E20	1.77	0.03	820	834	841	848	51	48	0.75	Churn
E21	1.17	0.05	783	793	793	800	64	61	0.82	**
E22	1.70	0.07	741	751	752	761	58	61	0.82	**
E23	1.13	0.02	1496	1510	1509	1524	48	45	0.73	Churn
E24	1.62	0.04	1586	1607	1606	1620	43	42	0.79	Churn
E25	1.162	0.05	1507	1516	1517	1524	55	54	0.75	Churn
E26	1.68	0.07	1358	1379	1378	1389	47	48	0.82	**

* Average insitu void fraction at the IA before Liquid breakthrough
** The authors are not wholly convinced this is churn flow at such gas void fractions.

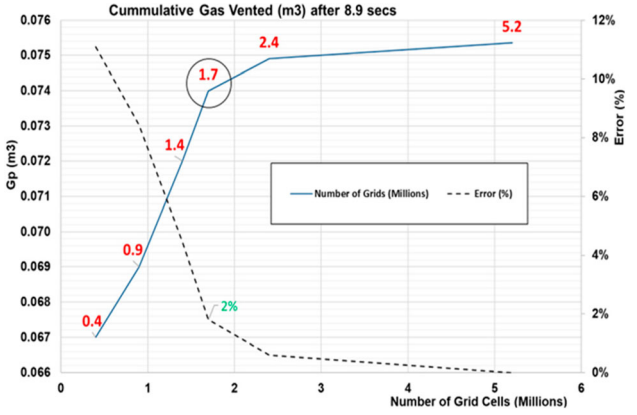


Figure 8. Mesh independence on Cumulative gas vented (Gp). Experiment 23.

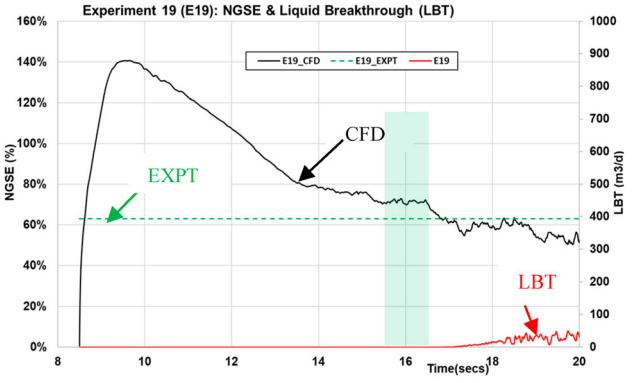


Figure 9. Experiment 19 and CFD results comparison.

the 5.2 million cells model to various mesh sizes. Figure 8 shows the trade-off between increasing the number of cells and the accuracy of the cumulative vent gas rate in comparison to the 5.2 million cells refined model after 8.9 s of simulation. Based on these comparisons, the 1.7 million cells model, which comprises 3 times fewer cells than the most refined model with a 2% error in cumulative gas vented (shown in Figure 8 with a black circle), was chosen as the most suitable mesh to achieve acceptable accuracy, while limiting CPU and computational time. Increasing the number of cells above 1.7 million did not make a significant difference on the cumulative gas result.

3.8. CFD results validation

Simulations were performed for all experiments identified in Table 2. A 20 s duration was deemed sufficient to ensure that the liquid level sufficiently increased to reach the Annulus-A outlet ('Liquid breakout'). The objective was to achieve a stable NGSE prior to liquid exiting the Annulus-A.

Alhanati (1993) reported challenges in achieving a completely stable liquid level in his experimental setup. Like our CFD simulations, his tests encountered a continuously rising liquid level within the annulus (Alhanati, 1993). In both cases, the data points were collected during the most stable or 'pseudo-stable' region observed, before liquid exited the Annulus-A.

To estimate the NGSE, Equation 9 was considered:

$$NGSE = \frac{Q_{gv}(Gas\ rate\ from\ Annulus - A)}{Q_{gt}(Inlet\ feed\ gas\ rate)} \quad (9)$$

Figures 9–16 show the NSGE (black curve) for all experiments after 8.5 s of opening the Annulus-A outlet valve. The caption on Figure 9, introduces the various curves: the green dashed line represents Alhanati's Experimental values (Alhanati, 1993) and the quantity of liquid (red curve) evacuating the annulus is defined as the liquid breakthrough rate (LBT). The green shaded box shows the selected NGSE data point.

As noticed in all experiments, as liquid breakthrough occurs (increasing liquid content in the model), the NGSE decreases. This is clearly seen after 14 s in Figure 11 (Experiment 21) and Figure 15 (Experiment 25). Such

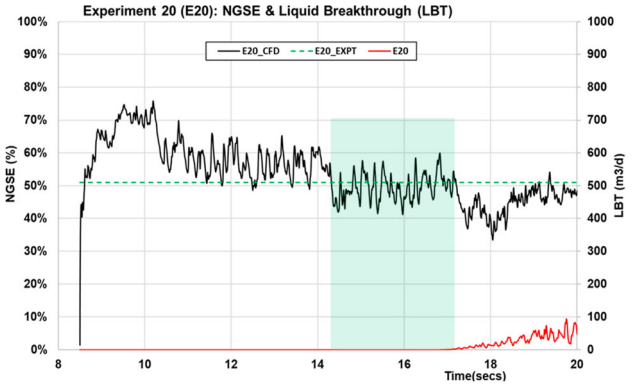


Figure 10. Experiment 20 and CFD results comparison.

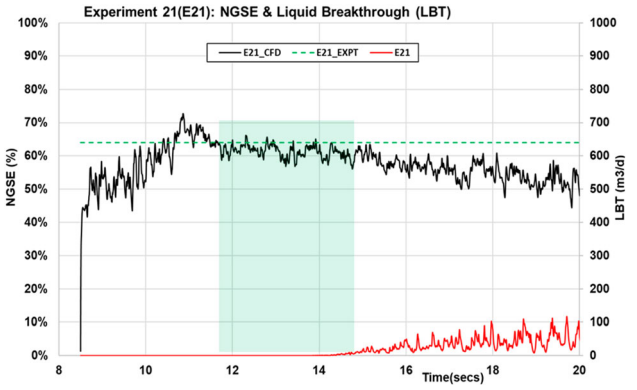


Figure 11. Experiment 21 and CFD results comparison.

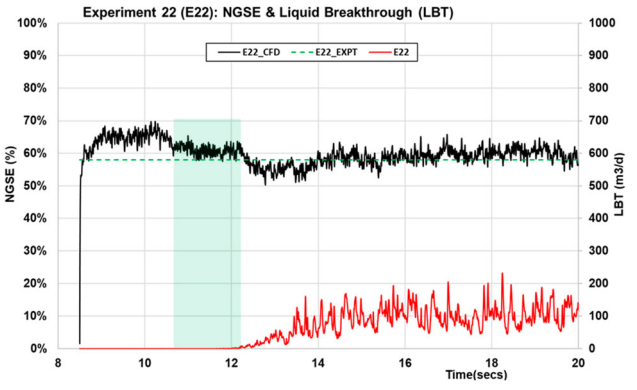


Figure 12. Experiment 22 and CFD results comparison.

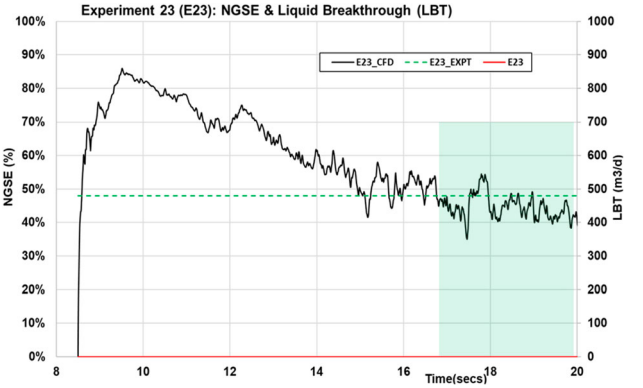


Figure 13. Experiment 23 and CFD results comparison.

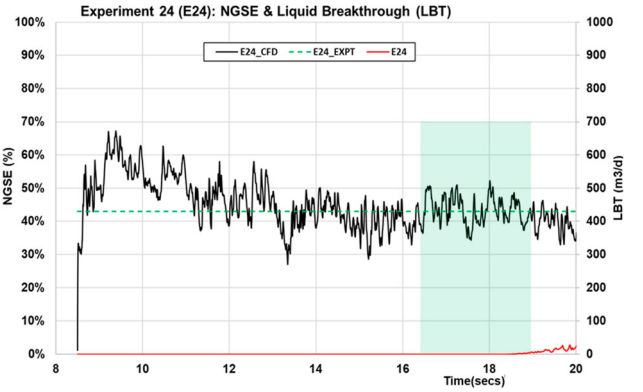


Figure 14. Experiment 24 and CFD results comparison.

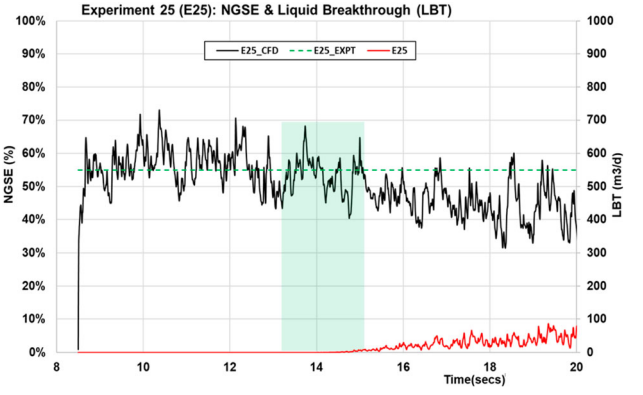


Figure 15. Experiment 25 and CFD results comparison.

behaviour aligns with experimental observations where an increase in the liquid content or liquid phase fraction decreases NGSE (Lackner, 1997; Harun et al., 2000).

Using Equation (10), a good agreement appears between CFD-based numerical results and the experimental/measured data from Alhanati (1993), with an average absolute error of less than 6% for all 8 experiments considered (average error between column H and I in Table 6). This provides confidence in the 1.7 million cells model and numerical settings for further sensitivity or parametric studies.

$$E_1 = \left[\frac{1}{N}\sum_{j=1}^{N} e_{\Gamma_i}\right] 100 \tag{10}$$

Table 6 summarizes the boundary conditions and results, showing a good match obtained from the numerical model. The parameters to match in comparison to the experiments are the pipe inlet pressure (Pip) and the NGSE (estimated from the Q_{gv}).

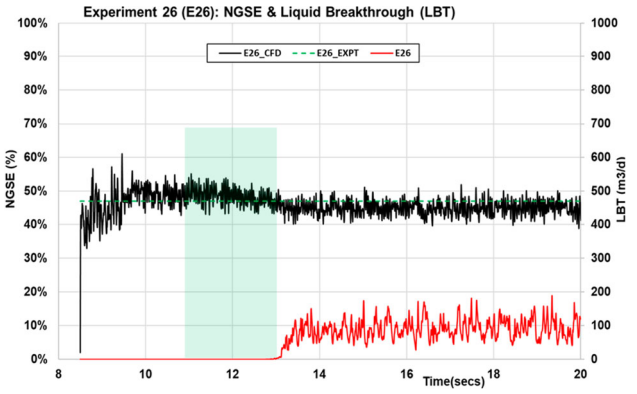


Figure 16. Experiment 26 and CFD results comparison.

This good match was achieved using the mass rates and pressure outlet boundary conditions respectively.

3.9. Flow regime identification at the IA

To identify the flow regime in the vicinity of the pump intake, the insitu gas void fraction was obtained numerically at the IA, for all eight experimental conditions (Figure 17B). The insitu void fraction at the IA is above 0.65 for all experiments. Based on these results, it appears that most (aside Experiment 21; 22 & 26) of Alhanati, 1993s experiments operated in the chaotic churn flow regime only, as similar gas void fraction plots obtained with CFD simulations of gas–liquid mixtures in the churn flow regime were obtained by Sun et al. (2019).

Identifying most of Alhanati's experiments at the IA as being in the churn flow regime, however, contradicts the literature, where past analytical research has identified these experiments to have operated in the slug or churn flow regimes (Marquez & Prado, 2007 ; Marquez & Prado, 2009). The type of flow investigated here is highly chaotic, the insitu void fractions in Table 6 are higher than published values for flow pattern criteria for slug flow (Ghiaasiaan, 2007) and with void fractions much higher than 0.52 for a churn flow regime (Hasan et al., 2007). The present authors thus believe that the chaotic churn flow regime dominated most of Alhanati's experiments and a complete steady state assumption considered by previous authors might not be entirely adequate for this flow regime.

Based on Figures 9–17, it can be established that most of Alhanati's experiments did not achieve complete stable conditions around the pump intake (i.e IA) before liquid break out from Annulus-A. Such chaotic, unstable conditions might be a contributing factor to the results for Cluster C in Figure 2, where the improved Marquez and Prado drift flux models showed a poor match, and approximately a 22% error.

As reported by Lima (2020), drift flux models are not the most appropriate models for the churn flow regime, however, most analytical formulations in the literature assume steady state conditions; which is also a limitation for this kind of highly instable and chaotic time-dependent flow regime.

4. Sensitivity analysis

To conduct the sensitivity analysis, experiment 23 was considered as the 'Base Case (BC)' model. The operating and boundary conditions for experiment 23 can be found in Tables 2 and 6.

Sensitivity studies were conducted for two categories:

(a) Fluid properties: surface tension, liquid density, liquid viscosity.
(b) Geometry: Annulus-A diameter (Casing ID – Tubing OD) and Pump Intake Port Flow Area.

The authors chose not to sensitize on pressure (Amrin F. Harun et al., 2000; Marquez & Prado, 2009) as it was obvious that increasing the back pressure prevents more gas from venting and hence decreases NGSE.

4.1. Surface tension

The surface tension appears in the terminal velocity equation (Equation 3). The surface tension for water and air used in the BC model was about 0.067 N/m. The typical surface tension of hydrocarbon oil and gas is estimated at about 0.020–0.030 N/m (Abdul-Majeed & Al-Soof, 2000). For the surface tension sensitivity analysis, 0.067 and 0.032 N/m were selected. The objective was to assess qualitatively a ∼50% reduction in the surface tension and its effect on the NGSE.

Figure 18 shows the results when the surface tension value is decreased by circa 50%. There is negligible difference seen in the NGSE (after 15s) as inertia forces dominate over surface tension forces. Similar experimental results were obtained by Lackner (1997) who reported that the surface tension had a minor influence on the NGSE after swapping the working fluids from water–air to mineral oil-air.

4.2. Liquid density

Typical liquid densities associated with oil field pumping can range from 1.00 g/cm3 (API gravity 10) to 0.87 g/cm3 (API gravity 32). Lighter densities are possible (Awadh & Al-Mimar, 2015; Khakimyanov & Khusainov, 2016). However, this study focuses on simulating a change from a heavy liquid 1.00 g/cm3 (10

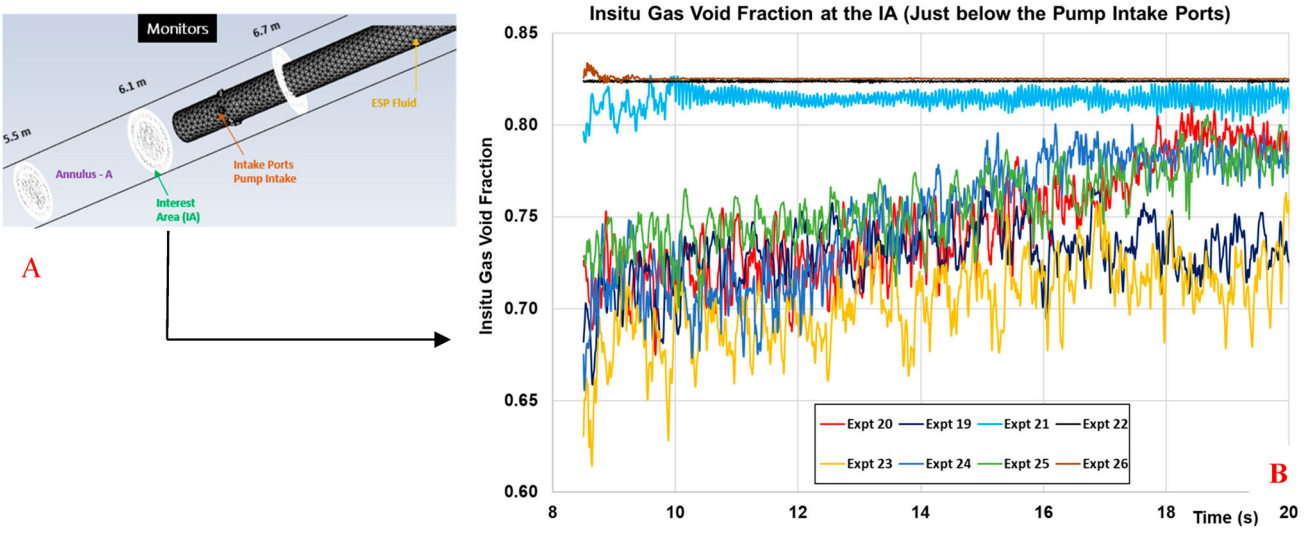


Figure 17. (A) Interest Area (IA) (B) Simulated Insitu Gas (air) void fraction at IA.

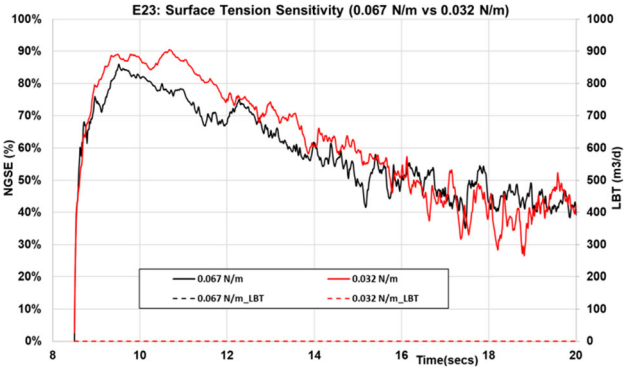


Figure 18. EXPT 23 Surface tension sensitivity.

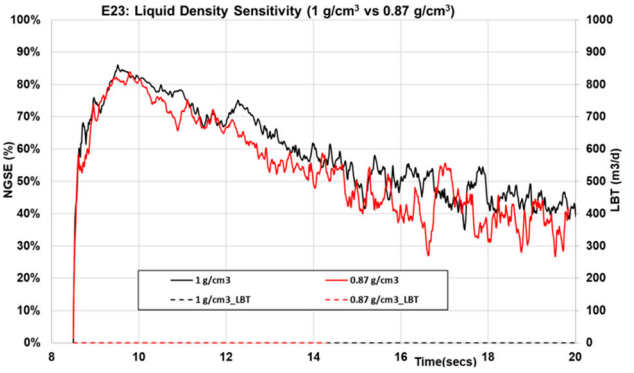


Figure 19. EXPT 23 Liquid density sensitivity.

API) to a light liquid 0.87 g/cm3 (32 API). Figure 19 shows a slight reduction in the NGSE with changes in liquid density. Again, similar results on liquid density were reported by Lackner (1997), where minor influences were noticed in the NGSE. Lackner's experimental results showed that within a liquid density of 10–32 API (1.00 g/cm3–0.87 g/cm3), there was no conclusive major influence on the NGSE during a dominated Newtonian/turbulent flow regime.

4.3. Liquid viscosity

ESPs are currently the most common artificial lift choices for operating in harsh oil and viscous environments (Guerrero-Sarabia & Fairuzov, 2006; Guarin Arenas et al., 2010; Bellary et al., 2017). The ESP can be exposed to viscous service, with the pumping of oil water emulsion or heavy oil viscosities as high as 1100 mPa·s at downhole reservoir conditions (Bhoendie et al., 2014).

Major flow regimes (slug, churn and annular) could also be experienced, even at high viscosity values above 500 mPa·s (Ribeiro et al., 2020). As noted previously, Lackner (1997) investigated experimentally the effects of the increase of liquid viscosity on the NGSE (at similar thermo-hydraulic conditions) but did not exceed 50 mPa·s. The effects of increasing the liquid viscosity on the NGSE were investigated through CFD in this work. The properties of water in the BC model were described with 1 mPa·s. and sensitivity studies were conducted on 10 and 100 mPa·s. liquid viscosity values while keeping other parameters constant.

Determining the Reynolds number for multiphase flows can be challenging. Although the slip improved (Ortiz-Vidal et al., 2014) and two-phase Reynolds number expressions can be used, the simplified no-slip mixture two-phase Reynolds number (Re2ph) flow method (Equation 11) was applied (Shannak, 2008; Shannak et al., 2010), which identified the 100 mPa·s viscosity values to be operating in a mixture of mostly laminar flow regime

Table 7. Estimated flow regime and assigned flow physics.

Sensitivity/Model	Shannak's Re_{2ph}	CFD model
1 mPa·s.	32861	k–ϵ
10 mPa·s.	3295	k–ω SST
100 mPa·s.	412	k–ω SST

around the pump intake.

$$Re_{2ph} = \frac{m_{2ph} D[x^2 + (1-x)^2 \rho_g/\rho_l]}{\mu_g x + \mu_l (1-x)\rho_g/\rho_l} \qquad (11)$$

where D is the diameter of the pipe, u_g and μ_l are the dynamic viscosities of the gas and liquid phases, respectively, and x is the quality of the flowing gas phase (ratio of gas mass rate to total mass rate).

It is expected that, as the liquid viscosity is increased from 1 mPa·s. to 100 mPa·s., the mixed flow will become non turbulent and the additional viscosity due to turbulence becomes more effective as shown by results from similar CFD studies (Okafor et al., 2021).

Based on the Reynolds expression of Shannak (2008), the mixture is described as follows through Table 7 in the vicinity of the IA:

Figure A2 presents in-situ gas void fraction and turbulent kinetic energy (TKE) data for the 100 mPa·s viscosity case at 8.5 s on the Y-Z plane. Notably, despite Shannak's model predicting laminar flow in Table 7, the TKE values remain above zero (at the intake area, IA), indicating the presence of some turbulence.

Furthermore, the TKE increases significantly after 9 metres, coinciding with a void fraction exceeding 0.8 (gas vent region). This reinforces the need for a robust turbulence model capable of handling gas-dominated cells.

The k-ϵ SST model was therefore chosen due to its ability to accurately allocate a representative turbulent viscosity and transition smoothly between viscous and fully turbulent regions. In areas where TKE approaches zero, the k-ϵ SST model is expected to minimize unnecessary dissipation rate addition.

Hence, for the viscosity sensitivity analysis, major changes regarding wall refinements (inflation layers) and flow regime (turbulence vs laminar) were considered.

For the 10 and 100 mPa·s cases, the turbulence model was changed from k–ϵ to k–ω SST with 'Low Reynolds Correction', as the magnitude of the viscous force gradually becomes dominant as viscosity increases.

The k–ω SST combines the k–ω formulation at the walls, and the k–ϵ formulation away from them (ANSYS, 2011). To meet the y+ requirements for the k–ω SST turbulence model, the mesh was further refined at the wall, and a y+ value less than 5 (Figure A3) was achieved for a mesh built with 20 inflation layers (3.6 million cells).

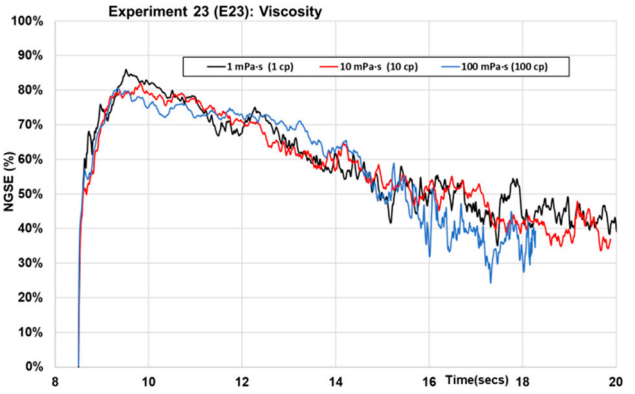


Figure 20. EXPT 23 Liquid viscosity sensitivity.

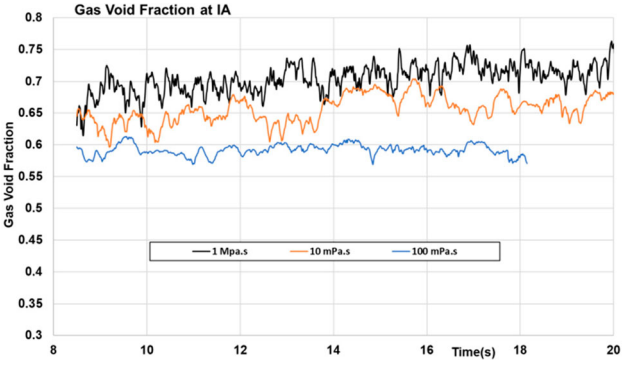


Figure 21. EXPT 23 Insitu air void fraction at IA (1, 10 and 100) mPa·s.

This wall-refined model is CPU expensive, and about 6 months were required for one simulation on 32 cores with a time step of 1 × 104 secs, to reach a total simulation time of 15.5 secs.

Figure 20 shows that the NGSE decreases as the liquid viscosity is increased. As liquid viscosity increases, the in-situ gas void fraction decreases, and this can be attributed to increased shear stress and liquid accumulation hindering gas mobility. Figure 21 shows the in-situ gas void fraction at the IA for 1 mPa·s,10, and 100 mPa·s. Similar void fraction behaviour was reported by Al-Ruhaimani et al. (2017) and Ribeiro et al. (2020) for experimental studies on gas void fraction at highly viscous liquids (100–580 mPa·s).

Most current ESP modelling software applying analytical methods for NGSE calculations (i.e. Equations 2 and 4), do not correct for viscous service. A key recommendation from the authors is to estimate the mixture two-phase Reynolds number using a method such as from Shannak (2008). If the estimated Re_{2ph} identifies a non-turbulent flow, then a correction for the drag and void fraction expression with the inclusion of the molecular viscosity is recommended (Okafor et al., 2021).

Table 8. Void fraction models vs CFD simulation.

Physical model	Class	Void fraction	Err %
CFD [Figure 21]		0.595	0
Lockhart and Martinelli (1949)	SR	0.641	7.7
Turner and Wallis (1965)	SR	0.304	48.9
CISE (Premoli, 1970)	SR	0.636	6.9
Woldesemayat and Ghajar (2007)	DFM	0.757	27.2
Ribeiro et al. (2020) [Equation 12]	SR	0.625	5.0

The rise velocity of gas bubbles is decreased with increased liquid viscosity, thereby reducing gas holdup. This effect is evident in Figure 21 and necessitates incorporating a void fraction expression in Equation (2) that accounts for increased viscosity. While existing correlations partially address this, they fall short in viscous conditions (Ribeiro et al., 2020).

Few correlations could adequately predict decreased gas void fraction with increasing liquid viscosity: slip ratio (SR) or drift flux (DFM). These models should include the liquid viscosity or the two-phase Reynolds number in the void fraction expression.

Table 8 demonstrates this concept. The CISE model (Premoli, 1970) and the Ribeiro et al. model (2020) (Equation 12) outperform the drift flux model from Woldesemayat and Ghajar (2007) when estimating the in-situ void fraction (for viscous service 100cp) in the heterogeneous churn flow. Based on these results, Equation (12) is recommended for in situ void fraction estimation needed for the NGSE calculations of Equation (2).

$$\alpha = \left[1 + 0.003\left(\frac{1-x}{x}\right)^{0.27}\left(\frac{\rho_g}{\rho_l}\right)^{-0.36}\left(\frac{\mu_l}{\mu_g}\right)^{0.212}\right]^{-1} \tag{12}$$

4.4. Turbulence and near wall treatment

The Bhagwat and Ghajar (2014) drift flux model (DFM) also holds promise, applicable for liquid viscosities of 0.1 mPa·s to 600 mPa·s (Ghiaasiaan, 2007). It includes the two-phase Reynolds number to estimate the two-phase distribution coefficient and should potentially lead to better performance than Woldesemayat and Ghajar (2007).

However, significant knowledge gaps remain regarding NGSE behaviour with viscous liquids and the effectiveness of corrective approaches. Current research, though valuable, is limited by model accuracy and data availability. Further studies are crucial, especially for bubble homogeneous flow regimes where submersible pumps encounter viscous multiphase environments.

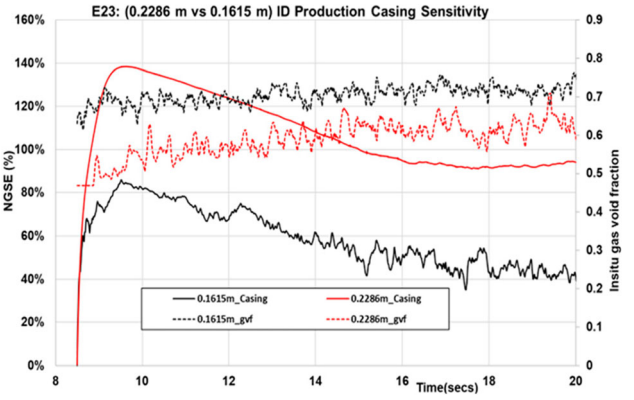


Figure 22. EXPT 23 Sensitivity on increasing Annulus-A diameter.

Table 9. Tubing sizes and annulus area increases.

	Production casing IDc (m)	Tubing ODt (m)	AHD (m)	Annulus flow area (m^2)
Case 1	0.1615	0.0890	0.0725	0.0140
Case 2	0.2286	0.0890	0.1396	0.0350
Case 3	0.2286	0.1400	0.0886	0.0260
% Annulus-A area Increase (Case 2 Vs Case 1)				144%
% Annulus-A area Increase (Case 2 Vs Case 3)				36%

4.5. Annulus diameter increase (Annulus space sensitivity)

Equation 4 allows us to investigate the Annular Hydraulic Diameter (AHD) – the space between tubing and casing – as a potential factor influencing NGSE. AHD (Equation 15) can be increased by enlarging the production casing inner diameter (IDc) or reducing the tubing outer diameter (ODt). Prior studies (Harun et al., 2000, 2001; Marquez & Prado, 2003) suggested that increasing AHD improves NGSE, typically by proposing a larger casing diameter. However, there is a lack of published experimental data to confirm the direct impact of casing size on NGSE.

$$AHD = ID_c - OD_t \tag{15}$$

Figure 22 presents CFD results on NGSE with a fixed downhole assembly (tubing diameter $\sim$ 0.089 m) but increasing casing diameter from 0.1615 m to 0.2286 m. This resulted in a significant NGSE increase from 45% to 92%. The findings also show a decrease in in-situ gas void fraction at the intake area (IA) due to a 144% increase in the total annulus flow area (Table 9). A larger annulus allows for a higher vent gas flow rate, consequently reducing gas holdup.

While previous studies proposed increasing production casing size to improve NGSE (Harun et al., 2000, 2001; Marquez & Prado, 2003), this approach is impractical for most ESP installations occurring during the mid-to-late production phase in wells with cemented casings (Camilleri & Gambier, 2013).

Our work presents a more practical alternative for existing wells. Table 9 (Case 2 vs Case 3) demonstrates the impact of tubing size on the AHD. In a well with a fixed casing diameter (0.2286 m), simply reducing the outer diameter of the tubing by 0.051 m (1 inch) leads to a significant 36% increase in the annulus area (normal to the flow path). This approach offers a feasible solution for enhancing NGSE in existing oil wells through a smaller tubing selection. A few extra ESP stages can be added to compensate for the increased frictional head and ensure production targets are met (Camilleri & Gambier, 2013). This strategy is easily implementable during the ESP design and installation phase for existing wells.

4.6. Pump intake port flow area (Port diameter)

Figure 1 illustrates the pump intake, the access point for fluids entering the ESP. Marquez and Prado (2003) introduced the concept of total intake port flow area (IPFA) as a parameter influencing NGSE through Equation (4). This parameter relates to the amount of gas drawn into the pump via the intake ports. A larger IPFA can lead to increased gas entrainment, reducing NGSE.

Figure 24(A) depicts a standard 400 series intake with six machined ports, each having a diameter of 17 mm. Figure 24(B) shows the corresponding CFD model replicating these features. Assuming all ports are active, the total IPFA is six times the area of a single port. ESP vendors categorize pump intakes by series. This strategy allows utilizing the same pump intake for various pump sizes within the same series. However, this practice can lead to mismatches between IPFA and pump capacity, potentially impacting NGSE.

Marquez and Prado (2003) suggested a positive correlation between total port size and NGSE, attributing it to fluid acceleration within smaller ports. However, this contradicts the assumption of steady-state flow in most analytical models, where acceleration effects become negligible once stable flow is established. To investigate this discrepancy, a sensitivity analysis using a VOF-based CFD model was conducted. This analysis focused on the impact of the total number of port holes available for flow intake, which ultimately affects the total IPFA. Two approaches can increase IPFA: increasing the number of ports while maintaining a constant diameter (explored here in Table 10) or increasing the diameter with the same number of ports.

Figure 23 reveals a critical relationship between total port flow area and NGSE. Our simulations demonstrate that increasing the port flow area reduces NGSE after 16 s due to more gas entrainment. Interestingly, an increase in NGSE is observed during the transient phase (before 16 s) with a larger port area (Marquez & Prado, 2003).

Table 10. Increased intake port flow area (Number of port holes increased) by keeping 17 mm port diameter constant.

Nos of ports	Average port diameter (mm)	Protruded area available for flow (mm^2)
6	16.76	1325.5
9	17.15	2081.3
12	16.84	2677.4

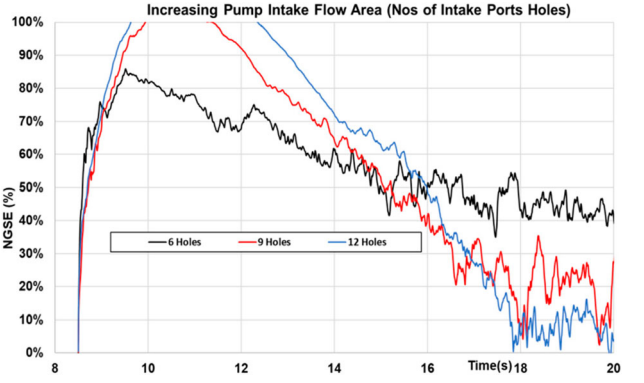


Figure 23. EXPT 23 Sensitivity on pump intake port hole flow area.

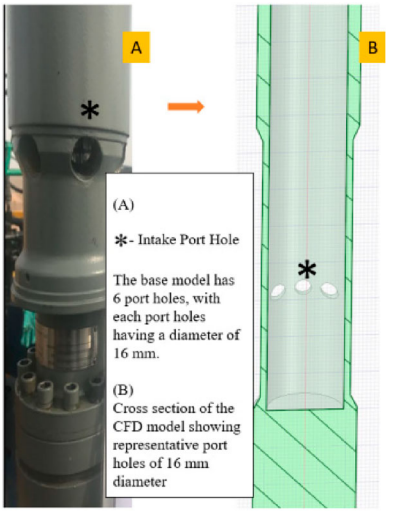


Figure 24. Intake Port Hole illustration in the CFD model.

These findings highlight the importance of considering port flow area's impact on NGSE during ESP design.

Current ESP designs prioritize factors like erosion prevention, capacity management, and manufacturing efficiency, often neglecting NGSE. Table 11 showcases two pumps from different series using the same Intake A (provided by an ESP vendor). Notably, Pump 2's Best Efficiency Point (BEP) flow rate is 41% higher than Pump 1's. While this common intake design simplifies inventory and shipping for vendors (as confirmed by a Middle Eastern oilfield case), it can negatively impact NGSE for smaller pumps. Intake A's Oversizing for Pump 1 and the Impact on NGSE: As shown in Figure 23, Intake

Table 11. Pumps of different sizes utilizing the same intake.

Pump ranges & intake								
Pump	Series	Downthrust limit (m^3/d)	Pump rate BEP (m^3/d)	Upthrust limit (m^3/d)	Intake	Port diameter (mm)	Number of holes	Total port flow area (mm^2)
1	362	413	588	715	A	16	10	2000
2	406	652	827	1002	A	16	10	2000

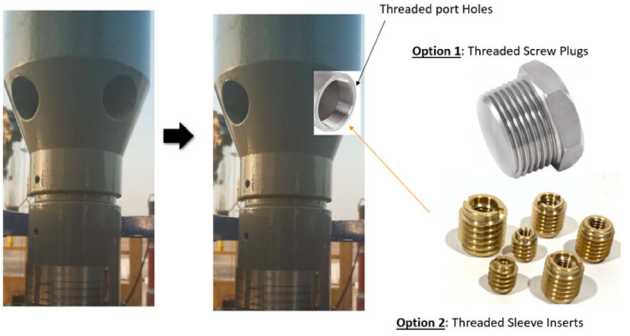


Figure 25. Intakes with threaded ports holes for adjustment: Screw plugs or threaded sleeves.

A is oversized for Pump 1. This excessive Intake Port Flow Area (IPFA) designed for Pump 2's higher flow rate hinders NGSE in Pump 1 (Figure 24).

A cost-effective approach to address this NGSE issue for Pump 1 using Intake A is to implement threaded port holes (Figure 25). This allows ESP vendors to maintain a standardized intake design while adjusting IPFA for different pumps. Either of the following is being proposed:

(a) *Dummy Screw Plugs*: Block unnecessary holes, converting the 9-hole system (Table 10) to a 6-hole system for Pump 1.
(b) *Threaded Sleeves*: Reduce the flow area within each port while maintaining all holes open for Pump 1.

These IPFA adjustments can be readily implemented by ESP installation crews on-site during well operations, eliminating the need for redesigning the intake itself. This approach offers a practical and cost-effective way for ESP vendors to improve NGSE and manage inventory for their clients.

We encourage ESP vendors to explore IPFA adjustment as a strategy to optimize NGSE for their clients. Further research is recommended to determine the optimal number of ports to be blocked or the degree of flow area reduction using threaded sleeves for various pump sizes within a series.

5. Conclusions and recommendations

5.1. Conclusions

This work highlights the advantages of CFD for advancing NGSE research in packer-less pumping wells with two-phase flows. Notably, our numerical model achieved excellent agreement with Alhanati's, 1993 experimental data (absolute error $< 6\%$). Furthermore, the model identified churn flow as the dominant regime in most experiments, contrasting with previous studies that suggested both slug and churn flow possibilities.

The observed chaotic and unsteady nature of the simulations in the churn flow regime suggests limitations in current analytical models, potentially explaining the observed 22% absolute error compared to measured NGSE data.

Fluid properties like surface tension and liquid density have minimal impact on the NGSE in turbulent flow. However, increasing the liquid viscosity reduces the in-situ gas void fraction and the NGSE, and such concerns ESPs handling viscous fluids (e.g. heavy oils or emulsions).

Void fraction models incorporating liquid viscosity are recommended for improved NGSE estimation accuracy. The Ribeiro et al. (2020) or CISE slip ratio model showed good agreement with void fraction CFD results for churn flow.

An innovative concept was proposed, discussing the maximization of the NGSE by increasing the AHD during the design and installation phases. A practical approach to maximize NGSE during ESP design involves increasing the Annulas-A Hydraulic Diameter (AHD) through a smaller tubing selection. Additional ESP stages can be incorporated to compensate for the friction head increase and meet production targets.

Minimizing the ESP intake size is crucial for maximizing NGSE and reducing gas entrainment. A larger total port flow area (more or larger ports) hinders NGSE. Therefore, port flow area should be a key consideration during ESP design, selection, and installation for NGSE optimization.

5.2. Recommendations

To achieve a more comprehensive understanding of NGSE dynamics across various multiphase flow conditions encountered in ESP well operations, future investigations using CFD simulations should explore NGSE behaviour in homogeneous regimes, such as bubble flow.

Current ESP modelling software for NGSE calculations in viscous services (heavy oil/emulsions) needs improvement. Void fraction models incorporating liquid

viscosity should be implemented to enhance NGSE accuracy. The validation/checking of this new approach with experimental or CFD data is crucial.

Slimmer downhole equipment, tubing, pumps section in existing production casing completed wells, should be promoted as much as possible in multiphase packerless pumping wells, without any detriment to production volume losses. Simulations showed that reducing the tubing size increases the annular hydraulic area and hence increases the NGSE.

ESP manufacturers and vendors should explore IPFA adjustment as a strategy to improve NGSE for their clients. Further research is recommended to determine the optimal number of ports to be blocked or the degree of flow area reduction using threaded sleeves.

CREDIT author statement

Okafor, C. Charles: Conceptualization, Methodology, Formal Analysis, Investigation, Writing Original Draft. **Verdin, G. Patrick:** Conceptualization, Writing, Review, Editing.

Disclosure statement

No potential conflict of interest was reported by the author(s).

References

Abdul-Majeed, G. H., & Al-Soof, N. B. A. (2000). Estimation of gas–oil surface tension. *Journal of Petroleum Science and Engineering*, *27*(3-4), 197–200. https://doi.org/10.1016/S0920-4105(00)00058-9

Al-Ruhaimani, F., Pereyra, E., Sarica, C., Al-Safran, E. M., & Torres, C. F. (2017). Experimental analysis and model evaluation of high-liquid-viscosity two-phase upward vertical pipe flow. *SPE Journal*, *22*(03), 712–735.

Alhanati, F. J. S. (1993). *Bottomhole gas separation efficiency in electrical submersible pump installations*. The University of Tulsa.

Alhanati, F. J. S., Sambangi, S. R., Doty, D. R., & Schmidt, Z. (1994, September). A simple model for the efficiency of rotary separators. In SPE Annual Technical Conference and Exhibition (pp. SPE-28525). SPE.

ANSYS Fluent, A.N.S.Y.S. (2011). Ansys fluent theory guide. Ansys Inc., USA, 15317, pp.724-746.

Anthony, O. I. (2017). *An integrated model for asset reliability, risk and production efficiency management in subsea oil and gas operations* [PhD thesis]. Newcastle University, UK.

Arenas, F. G., Garcia, C. A., Prada, C. A., Leon, E. C., & Santos, N. (2010, December). A new inflow model for extra-heavy crude oils: case study chichimene field, Colombia. In SPE Latin America and Caribbean Petroleum Engineering Conference (pp. SPE-138934). SPE.

Awadh, S. M., & Al-Mimar, H. (2015). Statistical analysis of the relations between API, specific gravity and sulfur content in the universal crude oil. *International Journal of Science and Research*, *4*(5), 1279–1284.

Bagci, A. S., Kece, M., & Nava, J. (2010, June). Challenges of using electrical submersible pump (ESP) in high free gas applications. In SPE International Oil and Gas Conference and Exhibition in China (pp. SPE-131760). SPE.

Bates, R., Cosad, C., Fielder, L., Kosmala, A., Hudson, S., Romero, G., & Shanmugam, V. (2004). Taking the pulse of producing wells—ESP surveillance. *Oilfield Review*, *16*(2), 16–25.

Bellary, S. A., Siddique, M. H., Samad, A., Sangwai, J. S., & Chon, B. (2017). Effects of crude oil-water emulsions at various water-cut on the performance of the centrifugal pump. *International Journal of Oil, Gas and Coal Technology*, *16*(1), 71–88. https://doi.org/10.1504/IJOGCT.2017.085998

Besagni, G., Inzoli, F., & Ziegenhein, T. (2018). Two-phase bubble columns: A comprehensive review. *ChemEngineering*, *2*(2), 13. https://doi.org/10.3390/chemengineering2020013

Bhagwat, S. M., & Ghajar, A. J. (2014). A flow pattern independent drift flux model based void fraction correlation for a wide range of gas-liquid two phase flow. *International Journal of Multiphase Flow*, *59*, 186–205.

Bhoendie, K. S., Moe Soe Let, K. P., Zitha, P. L., Pirlea, L., & Hebing, A. (2014, September). Case study of heavy-oil fluid characterization for gas EOR experiments: main challenges. In SPE Latin America and Caribbean Heavy and Extra Heavy Oil Conference (p. D031S021R003). SPE.

Caetano, E. F., Shoham, O., & Brill, J. P. (1992). Upward vertical two-phase flow through an annulus—Part I: Single-phase friction factor, Taylor bubble rise velocity, and flow pattern prediction.

Camilleri, L. (2020, October). Free Gas and ESP; Case Studies Illustrating the Difference Between Flowrate Oscillations, Gas Locking and Instability. In SPE Annual Technical Conference and Exhibition (p. D021S012R002). SPE.

Camilleri, L., & Gambier, P. (2013, March). Does your ESP Completion Architecture Meet All Your Production Requirements. In SPE Middle East Oil and Gas Show and Conference (pp. SPE-164249). SPE.

Ghiaasiaan, S. M. (2007). *Two-phase flow, boiling, and condensation: in conventional and miniature systems*. Cambridge University Press.

Gourma, M., & Verdin, P. G. (2016). Two-phase slug flows in helical pipes: Slug frequency alterations and helicity fluctuations. *International Journal of Multiphase Flow*, *86*, 10–20. https://doi.org/10.1016/j.ijmultiphaseflow.2016.07.013

Guerrero-Sarabia, I., & Fairuzov, Y. V. (2006, September). Startup of an ESP well producing heavy crude oil. In SPE Annual Technical Conference and Exhibition (pp. SPE-102953). SPE.

Guerrero, E., Muñoz, F., & Ratkovich, N. (2017). Comparison between Eulerian and vof models for two-phase flow assessment in vertical pipes. *CT&F-Ciencia, Tecnología y Futuro*, *7*(1), 73–84. https://doi.org/10.29047/01225383.66

Guo, R., Chen, Y., Waltrich, P. J., & Williams, W. C. (2018). An experimental investigation on flow pattern map and drift-flux model for co-current upward liquid-gas two-phase flow in narrow annuli. *Journal of Natural Gas Science and Engineering*, *51*, 65–72. https://doi.org/10.1016/j.jngse.2017.12.025

Harun, A. F., Prado, M. G., Serrano, J. C., & Doty, D. R. (2001, March). A mechanistic model to predict natural gas separation efficiency in inclined pumping wells. In SPE Oklahoma City Oil and Gas Symposium/Production and Operations Symposium (pp. SPE-67184). SPE.

Harun, A. F., Prado, M. G., Shirazi, S. A., & Doty, D. R. (2000, October). An improved model for predicting separation efficiency of a rotary gas separator in ESP systems. In SPE Annual Technical Conference and Exhibition (pp. SPE-63044). SPE.

Hasan, A. R., Kabir, C. S., & Sayarpour, M. (2007, November). A basic approach to wellbore two-phase flow modeling. In SPE Annual Technical Conference and Exhibition (pp. SPE-109868). SPE.

He, J., Hou, Q., Lian, J., Tijsseling, A. S., Bozkus, Z., Laanearu, J., & Lin, L. (2022). Three-dimensional CFD analysis of liquid slug acceleration and impact in a voided pipeline with end orifice. *Engineering Applications of Computational Fluid Mechanics*, *16*(1), 1444–1463. https://doi.org/10.1080/19942060.2022.2095440

Hibiki, T., & Ishii, M. (2002). Distribution parameter and drift velocity of drift-flux model in bubbly flow. *International Journal of Heat and Mass Transfer*, *45*(4), 707–721. https://doi.org/10.1016/S0017-9310(01)00195-8

Hua, G., Falcone, G., Teodoriu, C., & Morrison, G. (2012). Comparison of multiphase pumping technologies for subsea and downhole applications. *Oil and Gas Facilities*, *1*(01), 36–46.

Isao, K., & Mamoru, I. (1987). Drift flux model for large diameter pipe and new correlation for pool void fraction. *International Journal of Heat and Mass Transfer*, *30*(9), 1927–1939.

Itou, A., Nakanishi, T., Mizuguchi, T., Yoshida, M., & Saburi, T. (2005). High-performance parallel computing for Computational Fluid Dynamics (CFD) (Vol. 51, No. 156). Komatsu technical report.

Khakimyanov, M. I., & Khusainov, F. F. (2016). Research energy consumption of well electric submersible pumps for oil production. *International Journal of Business and Administrative Studies*, *2*(1), 1–5.

Krasnov, V. A., Litvinenko, K. V., & Khabibullin, R. A. (2014, October). An approach to account ESP head degradation in gassy well for ESP frequency optimization. In SPE Artificial Lift Conference and Exhibition-Americas? (p. D011S005R001). SPE.

Lackner, G. (1997). *The effect of viscosity on downhole gas separation in a Rotary Gas Seperator*. The University of Tulsa.

Lea, J. F., & Bearden, J. L. (1982). Effect of gaseous fluids on submersible pump performance. *Journal of Petroleum Technology*, *34*(12), 2922–2930. https://doi.org/10.2118/9218-PA

Liang, X., & El-Kadri, A. (2018, October). Factors affecting electrical submersible pump systems operation. In 2018 IEEE Electrical Power and Energy Conference (EPEC) (pp. 1-6). IEEE.

Lima, L. E. (2020). Application of the one-dimensional drift-flux model for numerical simulation of gas-liquid isothermal flows in vertical pipes: a mechanistic approach based on the flow pattern. *SN Applied Sciences*, *2*(4), 658. https://doi.org/10.1007/s42452-020-2440-x

Liu, B., & Prado, M. (2004, January). Modeling downhole natural separation using a bubble tracking method. In *ASME pressure vessels and piping conference* (Vol. 46806, pp. 3–10).

Liu, B., & Prado, M. (2005). Use of a bubble tracking method for prediction of downhole natural separation efficiency. *Journal of Pressure Vessel Technology*, *127*(4), 479–486.

Lockhart, R. W., & Martinelli, R. C. (1949). Proposed correlation of data for isothermal two-phase, two-component flow in pipes. *Chemical Engineering Progress*, *45*, 39–48.

Loyseau, X. F., & Verdin, P. G. (2016). Statistical model of transient particle dispersion and deposition in vertical pipes. *Journal of Aerosol Science*, *101*, 43–64. https://doi.org/10.1016/j.jaerosci.2016.07.013

Loyseau, X. F., Verdin, P. G., & Brown, L. D. (2018). Scale-up and turbulence modelling in pipes. *Journal of Petroleum Science and Engineering*, *162*, 1–11. https://doi.org/10.1016/j.petrol.2017.12.019

Marquez, R. A., & Prado, M. G. (2003, March). A new robust model for natural separation efficiency. In SPE Oklahoma City Oil and Gas Symposium/Production and Operations Symposium (pp. SPE-80922). SPE.

Márquez, R., & Prado, M. (2007). Mechanistic model for predicting downhole natural separation efficiency‘. *Revista Técnica de la Facultad de Ingeniería Universidad del Zulia*, *30*, 353–359.

Marquez, R., & Prado, M. G. (2009, January). Modelling downhole separation efficiency using a stream function approach. *International Conference on Offshore Mechanics and Arctic Engineering*, *43475*, 485–507.

Nedeltchev, S., & Schumpe, A. (2008). A new approach for the prediction of gas holdup in bubble columns operated under various pressures in the homogeneous regime. *Journal of Chemical Engineering of Japan*, *41*(8), 744–755. https://doi.org/10.1252/jcej.08we005

Okafor, C., Verdin, P., & Hart, P. (2021, September). CFD investigation of downhole natural gas separation efficiency in the churn flow regime. In SPE Gulf Coast Section Electric Submersible Pumps Symposium? (p. D042S005R002). SPE.

Ooo, B., & Purneftegas, R. N. (2008). *High GLR ESP technologies comparison field test results*. SPE paper 117414, The 2008 SPE Russian oil & Gas Technical Conference and Exhibition, Moscow (pp. 28–30).

Ortiz-Vidal, L. E., Mureithi, N., & Rodriguez, O. M. H. (2014). Two-phase friction factor in gas-liquid pipe flow. *Revista de Engenharia Térmica*, *13*(2), 81–88. https://doi.org/10.5380/reterm.v13i2.62101

Pessoa, R., & Prado, M. (2001, September). Experimental investigation of two-phase flow performance of electrical submersible pump stages. In SPE Annual Technical Conference and Exhibition (pp. SPE-71552). SPE.

Premoli, A. (1970). An empirical correlation for evaluating two-phase mixture density under adiabatic conditions. European Two-Phase Flow Group Meeting.

Ragab, A., & Brandstaetter, S. S. (2008). Multiphase flows in horizontal and inclined pipelines by cfd simulations multiphase flows in horizontal and inclined pipelines by CFD simulations.

Ribeiro, J. X., Liao, R., Aliyu, A. M., Baba, Y. D., Archibong-Eso, A., Ehinmowo, A., & Zilong, L. (2020). An assessment of gas void fraction prediction models in highly viscous liquid and gas two-phase vertical flows. *Journal of Natural Gas Science and Engineering*, *76*, 103107. https://doi.org/10.1016/j.jngse.2019.103107

Ribeiro, J. X., Liao, R., Aliyu, A. M., Baba, Y. D., Archibong-Eso, A., Ehinmowo, A., & Zilong, L. (2020). An assessment of gas void fraction prediction models in highly viscous liquid and gas two-phase vertical flows. *Journal of Natural Gas Science and Engineering*, *76*, 103107.

Sambangi, S. R. (1994). *Gas separation efficiency in electrical submersible pump installations with rotary gas separators* [MSc thesis]. The University of Tulsa, USA.

Serrano, J. C. (1999). *Natural separation efficiency in electrical submersible pump systems* [MSc thesis]. The University of Tulsa, USA.

Shakirov, A. M., & Petroleum, A. (2011). Middle east artificial lift forum MEALF-00098, an accurate model to predict natural separation efficiency based on common data.

Shannak, B. A. (2008). Frictional pressure drop of gas-liquid two-phase flow in pipes. *Nuclear engineering and design*, *238*(12), 3277–3284. https://doi.org/10.1016/j.nucengdes.2008.08.015

Shannak, B., Damseh, R., Al-Odat, M., Al-Shannag, M., & Azzi, A. (2010). Two-phase flow through corrugated U-tube. *Proceedings of the Institution of Mechanical Engineers, Part C: Journal of Mechanical Engineering Science*, *224*(11), 2408–2417. https://doi.org/10.1243/09544062JMES1871

Shi, H., Holmes, J. A., Durlofsky, L. J., Aziz, K., Diaz, L. R., Alkaya, B., & Oddie, G. (2005). Drift-flux modeling of two-phase flow in wellbores. *Spe Journal*, *10*(01), 24–33. https://doi.org/10.2118/84228-PA

Sun, C., Ning, Z., Qiao, X., Lv, M., Fu, J., Zhao, J., & Wang, X. (2019). Numerical simulation of gas–liquid flow behavior in the nozzle exit region of an effervescent atomizer. *International Journal of Spray and Combustion Dynamics*, *11*, 1–19.

Turner, J. M., & Wallis, G. B. (1965). *The separate-cylinders model of two-phase flow*. Paper no. NYO-3114-6, Thayer's School Engineering, Dartmouth College, Hanover, NH, USA.

Wilson, B. L. (1994, September). Esp gas separator's effect on run life. In SPE Annual Technical Conference and Exhibition (pp. SPE-28526). SPE.

Woldesemayat, M. A., & Ghajar, A. J. (2007). Comparison of void fraction correlations for different flow patterns in horizontal and upward inclined pipes. *International Journal of Multiphase Flow*, *33*(4), 347–370.

Zhu, J., & Zhang, H. Q. (2018). A review of experiments and modeling of gas-liquid flow in electrical submersible pumps. *Energies*, *11*(1), 180. https://doi.org/10.3390/en11010180

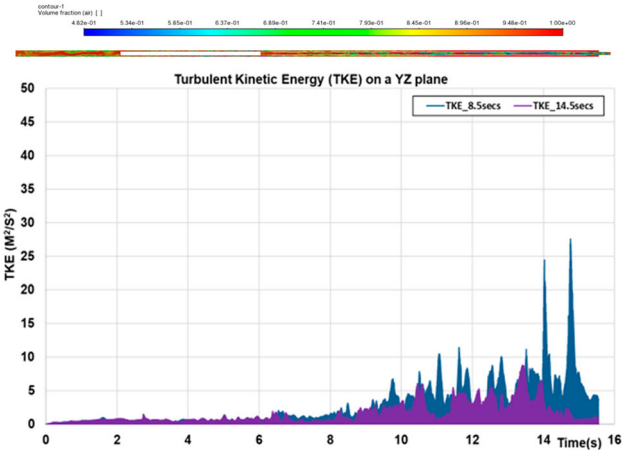


Figure A2. (Above) Insitu gas void fraction on the YZ plane for the 100mPas liquid viscosity case. (Below), Turbulent kinetic energy on a YZ plane for 100mPa.s.

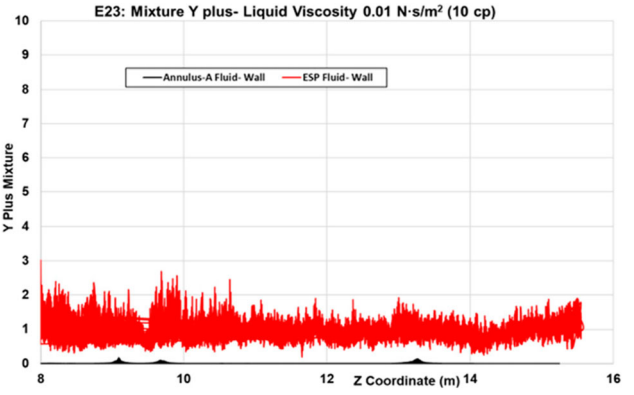


Figure A3. Mixture Y+: 10 mPa·s (10 cp).

Data availability statement		
Availability of data	Location	Policy
Data openly available in a public repository that issues datasets with DOIs	The data that support the findings of this study are openly available in OnePetro at https://doi.org/10.2118/28525-MS, reference number SPE-28525-MS	All

Appendix A

A.1 Standard k – ϵ two-equation turbulence model: ANSYS Fluent theory guide (ANSYS, 2011)

$$\frac{\partial(\rho_m k)}{\partial_t} + \frac{\partial(\rho_m k \mu_i)}{\partial x_i} = \frac{\partial}{\partial x_j}\left[\left(\mu_m + \frac{\mu_t}{\sigma_k}\right)\frac{\partial k}{\partial x_j}\right] + G_k + G_b - \rho_m \varepsilon - Y_M + S_k$$

$$\frac{\partial(\rho_m \varepsilon)}{\partial_t} + \frac{\partial(\rho_m \varepsilon \mu_i)}{\partial x_i} = \frac{\partial}{\partial x_j}\left[\left(\mu_m + \frac{\mu_t}{\sigma_\varepsilon}\right)\frac{\partial \varepsilon}{\partial x_j}\right] + C_{1\varepsilon}\frac{\varepsilon}{k}(G_k + C_{3\varepsilon}G_b) - C_{2\varepsilon}\rho_m\frac{\varepsilon^2}{k} + S_\varepsilon$$

$$\mu_t = C_\mu \rho_m \frac{k^2}{\varepsilon}$$



https://dspace.org/

3D computational fluid dynamics analysis of natural gas separation efficiency in multiphase pumping wells with heterogeneous flow regime

Okafor, Charles C.; Verdin, Patrick G.

2024-12-31
Taylor and Francis
https://doi.org/10.1080/19942060.2024.2395452
Okafor CC, Verdin PG. (2024) 3D computational fluid dynamics analysis of natural gas separation efficiency in multiphase pumping wells with heterogeneous flow regime. Engineering Applications of Computational Fluid Mechanics, Volume 18, Issue 1, 2024, Article number 2395452

Downloaded from a DSpace repository. https://dspace.org/